Cell Genomics

Article

ABCA7-dependent induction of neuropeptide Y is required for synaptic resilience in Alzheimer's disease through BDNF/NGFR signaling

Graphical abstract

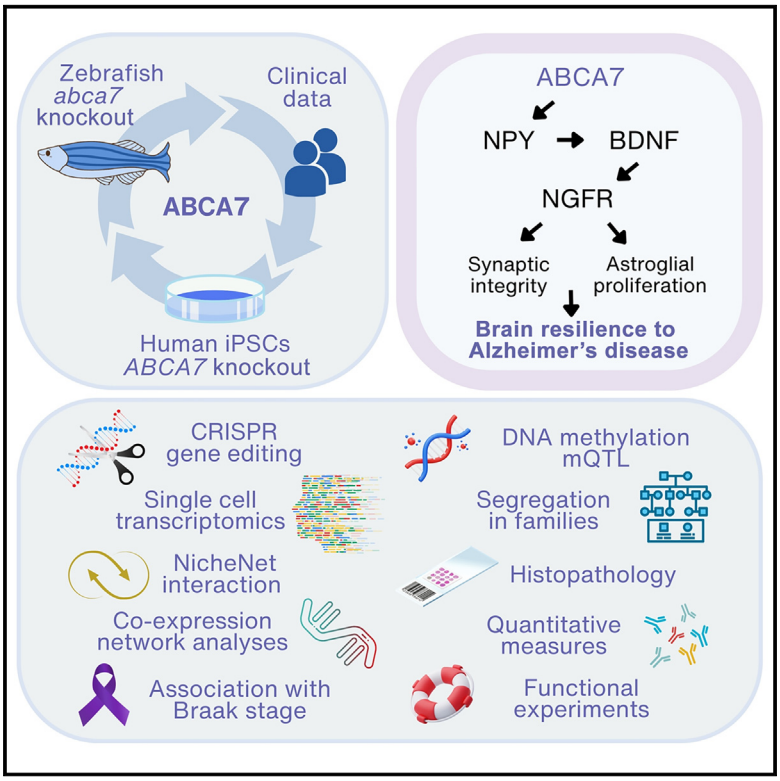

Highlights

- *ABCA7* knockout in zebrafish mimics Alzheimer's disease (AD) pathology
- Loss of *ABCA7* reduces neuropeptide Y (NPY) in zebrafish and humans
- NPY and BDNF signaling axis is essential for maintaining synaptic integrity in AD
- Zebrafish reveals *ABCA7*-dependent resilience mechanisms conserved in humans

Authors

Hüseyin Tayran, Elanur Yilmaz, Prabesh Bhattarai, ..., Nilüfer Ertekin-Taner, Richard Mayeux, Caghan Kizil

Correspondence

ck2893@cumc.columbia.edu

In brief

In this study, Tayran et al. investigate the role of *ABCA7*, certain genetic variants of which act as risk factors for Alzheimer's disease (AD), using a zebrafish AD model. They demonstrate that *ABCA7*-dependent induction of neuropeptide Y (NPY) and BDNF signaling is crucial for maintaining key resilience processes including synaptic integrity and astroglial proliferation. The findings uncover a previously unidentified mechanism by which brain resilience is impaired in AD patients and identify potential therapeutic targets to mitigate AD pathology.

Tayran et al., 2024, Cell Genomics *4*, 100642
September 11, 2024
https://doi.org/10.1016/j.xgen.2024.100642

CellPress

Cell Genomics

CellPress
OPEN ACCESS

Article

ABCA7-dependent induction of neuropeptide Y is required for synaptic resilience in Alzheimer's disease through BDNF/NGFR signaling

Hüseyin Tayran,[1,2,13] Elanur Yilmaz,[1,2,13] Prabesh Bhattarai,[1,2,13] Yuhao Min,[3] Xue Wang,[4] Yiyi Ma,[2] Ni Wang,[3] Inyoung Jeong,[5] Nastasia Nelson,[1,2] Nada Kassara,[1] Mehmet Ilyas Cosacak,[6] Ruya Merve Dogru,[1] Dolly Reyes-Dumeyer,[1,2,7] Jakob Mørkved Stenersen,[5] Joseph S. Reddy,[3] Min Qiao,[1,2,7] Delaney Flaherty,[1,9] Tamil Iniyan Gunasekaran,[1,2,7] Zikun Yang,[1,2,7] Nathalie Jurisch-Yaksi,[5] Andrew F. Teich,[1,2,9] Takahisa Kanekiyo,[3,8] Giuseppe Tosto,[1,2,7] Badri N. Vardarajan,[1,2,7] Özkan İş,[3] Nilüfer Ertekin-Taner,[3,10] Richard Mayeux,[1,2,7,11,12] and Caghan Kizil[1,2,7,14,*]

[1]The Taub Institute for Research on Alzheimer's Disease and the Aging Brain, Columbia University Irving Medical Center, Columbia University, New York, NY 10032, USA
[2]Department of Neurology, Columbia University Irving Medical Center, Columbia University, New York, NY 10032, USA
[3]Department of Neuroscience, Mayo Clinic Florida, Jacksonville, FL 32224, USA
[4]Department of Quantitative Health Sciences, Mayo Clinic Florida, Jacksonville, FL 32224, USA
[5]Department of Clinical and Molecular Medicine, Norwegian University of Science and Technology, Trondheim, Norway
[6]German Center for Neurodegenerative Diseases (DZNE), Tatzberg 41, 01307 Dresden, Germany
[7]The Gertrude H. Sergievsky Center, College of Physicians and Surgeons, Columbia University Irving Medical Center, Columbia University, 630 West 168th Street, New York, NY 10032, USA
[8]Center for Regenerative Biotherapeutics, Mayo Clinic, Jacksonville, FL 32224, USA
[9]Department of Pathology and Cell Biology, Columbia University Irving Medical Center, Columbia University, New York, NY 10032, USA
[10]Department of Neurology, Mayo Clinic Florida, Jacksonville, FL 32224, USA
[11]Department of Psychiatry, College of Physicians and Surgeons, Columbia University Irving Medical Center, Columbia University, 1051 Riverside Drive, New York, NY 10032, USA
[12]Department of Epidemiology, Mailman School of Public Health, Columbia University Irving Medical Center, Columbia University, 722 W. 168th St., New York, NY 10032, USA
[13]These authors contributed equally
[14]Lead contact
*Correspondence: ck2893@cumc.columbia.edu
https://doi.org/10.1016/j.xgen.2024.100642

SUMMARY

Genetic variants in *ABCA7*, an Alzheimer's disease (AD)-associated gene, elevate AD risk, yet its functional relevance to the etiology is unclear. We generated a CRISPR-Cas9-mediated *abca7* knockout zebrafish to explore *ABCA7*'s role in AD. Single-cell transcriptomics in heterozygous *abca7*$^{+/-}$ knockout combined with Aβ42 toxicity revealed that *ABCA7* is crucial for neuropeptide Y (*NPY*), brain-derived neurotrophic factor (*BDNF*), and nerve growth factor receptor (*NGFR*) expressions, which are crucial for synaptic integrity, astroglial proliferation, and microglial prevalence. Impaired *NPY* induction decreased *BDNF* and synaptic density, which are rescuable with ectopic NPY. In induced pluripotent stem cell-derived human neurons exposed to Aβ42, *ABCA7*$^{-/-}$ suppresses *NPY*. Clinical data showed reduced *NPY* in AD correlated with elevated Braak stages, genetic variants in *NPY* associated with AD, and epigenetic changes in *NPY*, *NGFR*, and *BDNF* promoters linked to *ABCA7* variants. Therefore, ABCA7-dependent NPY signaling via BDNF-NGFR maintains synaptic integrity, implicating its impairment in increased AD risk through reduced brain resilience.

INTRODUCTION

Alzheimer's disease (AD), a complex and progressive neurodegenerative disorder, continues to present a formidable challenge to the society. This currently incurable condition, characterized by cognitive decline, memory loss, and impaired daily functioning, has spurred large research efforts aimed at elucidating its underlying mechanisms. Among the multifaceted factors implicated in AD etiology, genetic variations have emerged as key players, offering insights into potential avenues of therapeutic exploration.[1–6] Despite the growing body of genetic evidence, the specific functions and mechanisms through which these genetic variations exert their influence remain a subject of ongoing investigation.[1,2,5,7] While genome-wide association studies have provided significant data linking certain candidate genes to AD susceptibility, deciphering the mechanistic roles of these genes demands scrutiny of their functional significance, which would be facilitated by disease-mimetic representative animal models.

Organisms that share conserved genetic elements with humans offer a valuable platform for robust functional analysis. We developed a zebrafish model of amyloid toxicity that shows strong parallels in the cellular and molecular readouts of the disease, including vascular perturbations, neurodegeneration, and immune reaction.[8–15] This model has enabled functional investigation of AD genetic variants[6,16–19] and investigation of new active and potent pharmacological agents.[8,20–23] One of the key strengths of the zebrafish is its remarkable neuroregenerative ability after amyloid toxicity, which involves activation of molecular mechanisms that govern astroglial proliferation.[15,24–28] Translational approaches that activate the molecular mechanisms in zebrafish to counteract amyloid toxicity through enhanced neurogenesis led to reduction of AD pathology in this model system.[29–33] Therefore, zebrafish can serve as a useful *in vivo* translational and functional research tool for investigating the synaptic integrity and resilience mechanisms in AD.

Multiple studies have indicated that both common and rare variants in *ABCA7* are strongly and consistently associated with AD risk and endophenotypes across different ethnic groups.[34–45] *ABCA7* encodes a transmembrane transporter with a demonstrated impact on lipid transport, a process integral to cellular membrane dynamics and overall homeostasis.[34,37,44,46–48] By facilitating the movement of lipids across cellular membranes, ABCA7 influences a range of cellular processes, including those vital for neuronal function and synaptic plasticity.[37,46,49–51] ABCA7 also modulates Aβ metabolism, a process central to the formation of the characteristic neuritic plaques observed in AD.[45,51] These underscore the significance of ABCA7 in orchestrating cellular mechanisms involved in AD pathogenesis; however, its range of functions and mechanistic relevance remain incompletely defined. This study was designed to explore the uncharted roles of ABCA7 using a multidisciplinary approach that leverages data from zebrafish models, human subjects, and patient-derived induced pluripotent stem cells (iPSCs).

RESULTS

abca7 knockout affects the astroglial proliferation, synaptic density, and microglia following amyloid toxicity

To determine the effects of heterozygous deletion of *abca7* in the zebrafish brain, we generated a truncated version of the gene by deleting 44.5 kb of genomic region between exon 13 and exon 46 with CRISPR-Cas9-based gene editing (Figures 1A and 1B; Table S1; Data S1). This genomic deletion removes the protein domains after the second transmembrane domain including the ATPase and transporter domains, generating a null allele, similar to the human frameshift variation that is associated with AD risk.[37,52–54] This deletion is transmitted in Mendelian ratios (Figure 1C), genetically stable in adults (Figure 1D), and *abca7*$^{+/-}$ animals are viable and fertile. To investigate the adult brains of *abca7*$^{+/-}$ zebrafish, we performed immunostaining for astroglial (GS), microglial (L-plastin), synaptic (SV2), and proliferation (proliferating cell nuclear antigen [PCNA]) markers in the presence or absence of Aβ42 toxicity (Figures 1E and 1F). These markers were selected because of their relevance to the neuropathology of AD: GS for its role in astroglial response, L-plastin for microglial activity indicative of brain immune response, SV2 for synaptic integrity reflecting neural communication, and PCNA for cellular proliferation indicative of regeneration and repair mechanisms. Compared to wild-type animals, *abca7*$^{+/-}$ knockouts did not change astroglial proliferation and microglial numbers but reduced synaptic integrity (Figure 1G). After Aβ42 was introduced through cerebroventricular microinjection, wild-type animals increased astroglial proliferation and the number of microglia, while synaptic integrity was reduced (Figure 1G). *abca7*$^{+/-}$ knockouts failed to increase astroglial proliferation and microglial numbers, and further reduced the synaptic integrity (Figures 1G and S1; Data S1). These results suggest that *abca7* gene function is related to Aβ42-induced astroglial proliferation, synaptic integrity, and microglial activity.

abca7 is required for neuropeptide Y (*npy*) expression in response to amyloid

We performed single-cell transcriptomics in wild-type/PBS-injected, wild-type/Aβ42-injected, *abca7*$^{+/-}$/PBS-injected, and *abca7*$^{+/-}$/Aβ42-injected zebrafish (Figure 2A) to investigate the molecular basis of the *abca7*-dependent cellular changes. After quality control for mitochondrial gene ratios, abundance of ribosomal gene expression, distribution of the number of genes per cell, and number of reads per cell (Figures 2B and 2C), we determined the main cell-type markers to categorize the 36 cell clusters (Figure 2D), which include 11 neuronal, 4 astroglial, 4 microglial, 3 immature neuronal, 2 immune, 2 vascular smooth muscle cell, 2 endothelial, 2 oligodendrocyte progenitor, 3 uncategorized, 1 neuroblast, 1 oligodendrocytic, and 1 pericytic cell cluster (Figures 2D, S2A, and S2B). In total, 50,691 cells passed the quality criteria and were clustered in the final uniform manifold approximation and projection (UMAP) (Figure 2E). 57.82% of the cells were neurons, followed by 10.35% astroglia and 5.88% microglia (Figure 2E). The number of cells sequenced in all clusters (Figure 2F) and the number of cells sequenced per cell type in four samples combined and individually (Figures 2G and S2C) were sufficient in terms of the sample size (SCOPIT[55] and detection power for differential expression, scPower[56], as per analyses with the following parameters: cell-type frequency, 0.3; multiple testing method, false discovery rate [FDR]; *p* value, 0.05; mapping efficiency, 0.8; minimum number of UMIs [unique molecular identifiers] per gene, 3; which resulted in a detection power of 0.901 should 2,057 cells be sequenced per sample with a read depth of 928,571). Since our sequencing parameters fulfill these criteria for reliable detection and differential expression power (Figures 2 and S2), we proceeded with the analyses of cell clusters.

To determine the differentially expressed genes, we used FindMarkers functions of Seurat and found the genes that are differentially expressed in *abca7*$^{+/-}$ animals in comparison to wild types in the presence of Aβ42 (*abca7*$^{+/-}$ vs. wild type and *abca7*$^{+/-}$/Aβ42 vs. wild type/Aβ42) (Figure 2H and Data S2). Selection of the top enriched gene ontology (GO) terms in every cell type showed that NPY signaling and neurogenesis were highly represented in astroglia, excitatory and inhibitory neurons, oligodendrocyte precursor cells, and pericytes (Figure 2I). Interestingly, in oligodendrocytes (ODs), these processes were not

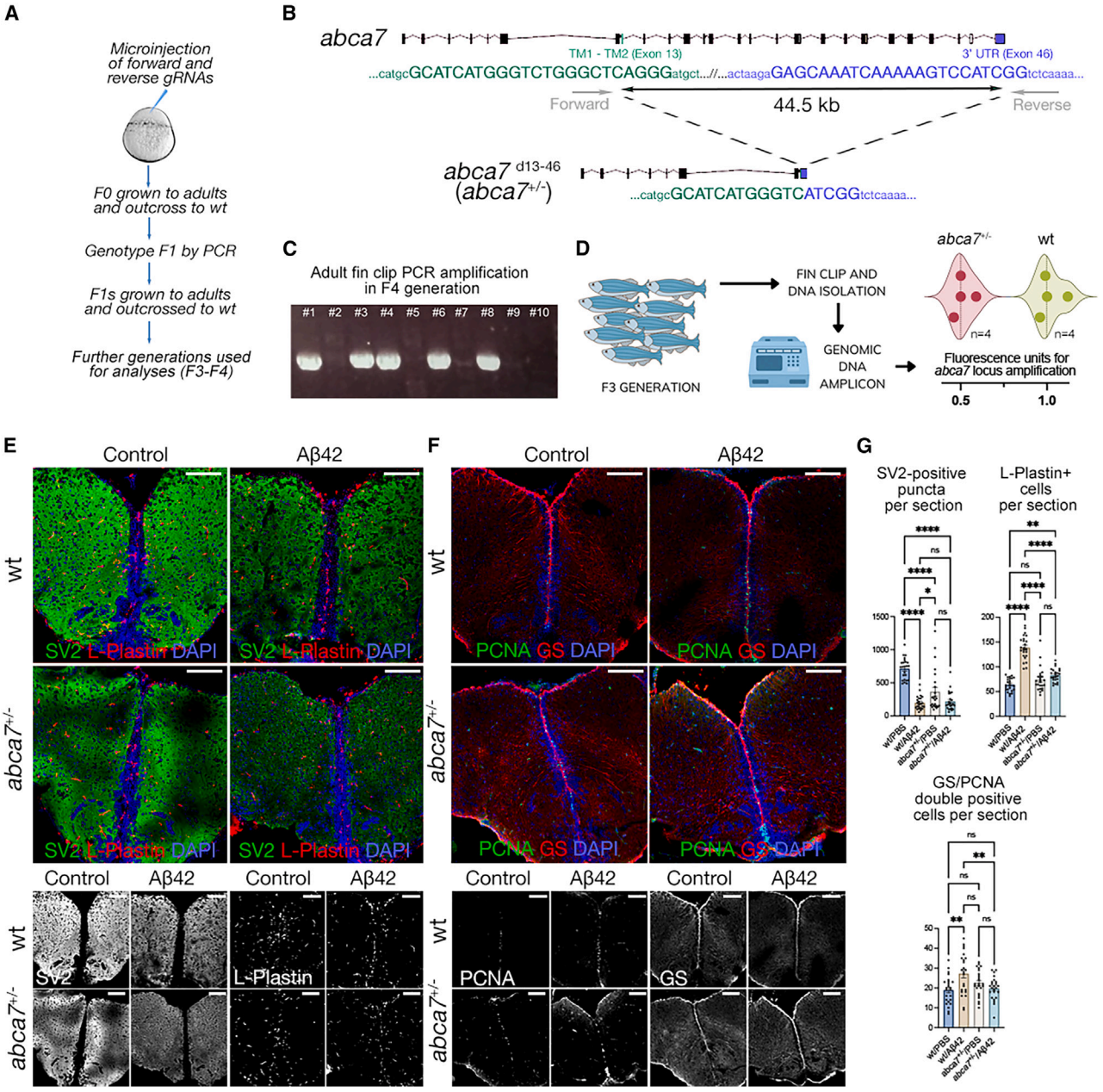

Figure 1. *abca7* is required for synaptic integrity, microglial prevalence, and astroglial proliferation in zebrafish

(A) Schematic view of generating *abca7* knockout line.

(B) 44.5-kb deletion in *abca7* gene.

(C) Representative genotyping PCR gel from F4 generation where positive bands indicate the deletion. Every column is one adult fin-clip DNA sample amplified with the forward and reverse primers in (B).

(D) Genotyping results with genomic DNA qPCR in F3 adults. Eight animals (four wild-type and four heterozygous deletions) were used. Heterozygous deletions show reduced amplification (lower fluorescence). Results depicted as violin plots and individual values.

(E) Immunofluorescence (IF) for SV2 (green) and L-plastin (red) with DAPI counterstain in wild type and *abca7*$^{+/-}$ with and without Aβ42. Black and white panels indicate individual fluorescent channels.

(F) IF for PCNA (green) and GS (red) with DAPI counterstain in wild type and *abca7*$^{+/-}$ with and without Aβ42. Black and white panels indicate individual fluorescent channels.

(G) Quantification of SV2-positive synaptic puncta, number of microglial cells, and number of proliferating astroglia.

One-way ANOVA with Tukey's multiple comparison test was used for statistical analyses. $n = 4$ animals from both sexes with 24 brain sections per group. $^{*}p < 0.0332$, $^{**}p < 0.0021$, $^{***}p < 0.0002$, $^{****}p < 0.0001$; not significant (ns), $p > 0.0332$. Scale bars, 100 μm. See also Figures S1 and S4, Data S1, and Table S1.

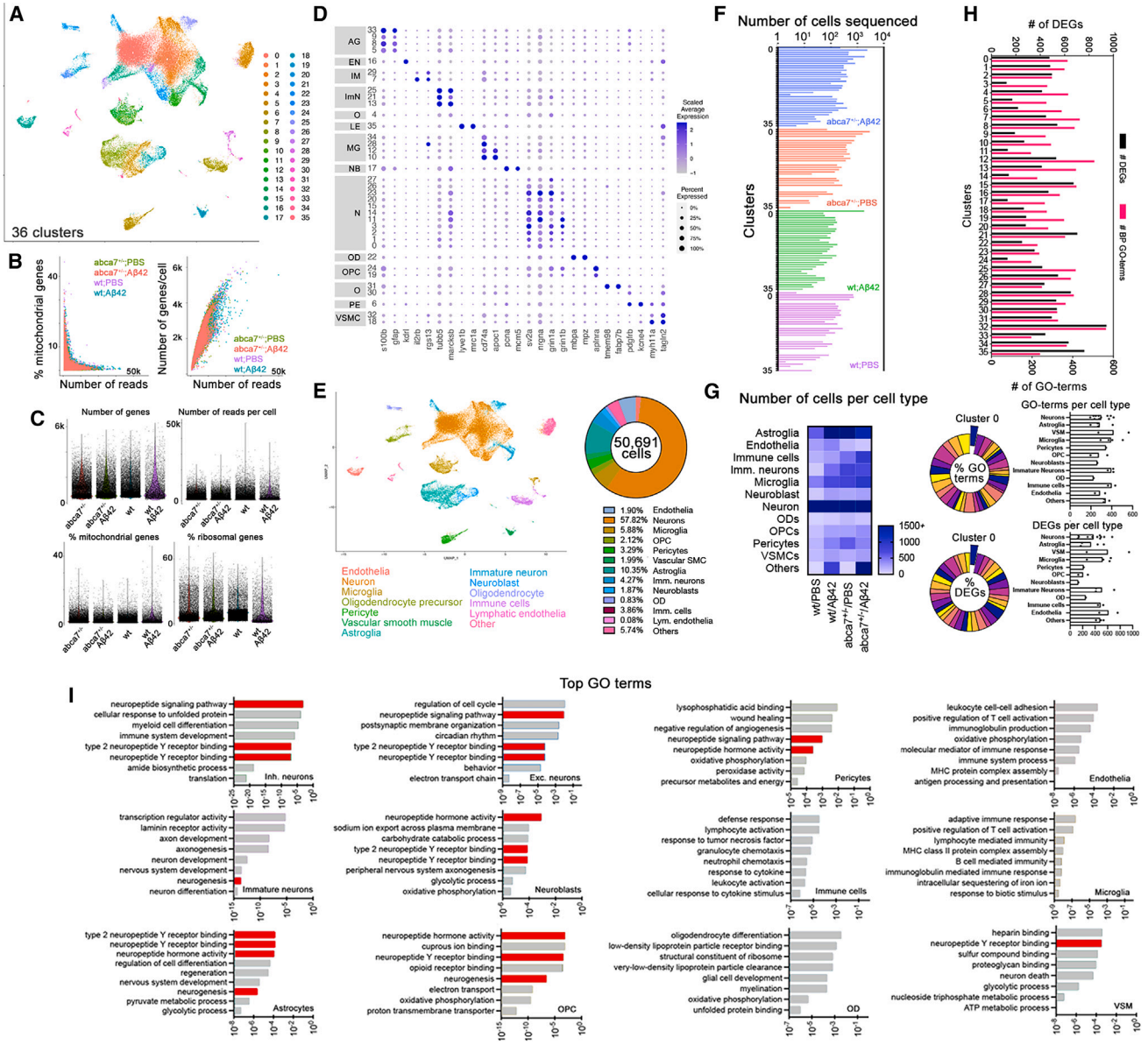

Figure 2. Single-cell transcriptomics in *abca7* knockout zebrafish

(A) Combined UMAP plot for single-cell transcriptomics from wild-type + PBS, wild-type + Aβ42, *abca7*$^{+/-}$ + PBS, and *abca7*$^{+/-}$ + Aβ42 samples; 36 cell clusters were identified.

(B) Percentage of mitochondrial counts and number of genes per cell.

(C) Number of genes, number of reads per cell, percentage of mitochondrial gene expression, and percentage of ribosomal genes in every sample.

(D) Dotplot for cell-type markers identify distinct cell types.

(E) UMAP plot classifying cell types and their percent prevalence in a total of 50,691 cells sequenced.

(F) Distribution of the number of cells sequenced in all 36 clusters in every sample.

(G) Heatmap showing the number of sequenced cells per cell type.

(H) Number of differentially expressed genes (DEGs, black) and gene ontology (GO) terms related to biological processes (magenta) between wild-type + Aβ42 and *abca7*$^{+/-}$ + Aβ42 samples. Lower panels indicate pie chart of the percentage of GO terms and DEGs per cluster between wild-type + Aβ42 and *abca7*$^{+/-}$ + Aβ42 samples, and the numbers of GO terms and DEGs per cell type as bar graphs.

(I) Tally for top GO terms in distinct cell types. Neuropeptide signaling pathway and neurogenesis are enriched in neurons, neuroblasts, astroglia, oligodendrocyte progenitors, and vascular smooth muscle cells.

See also Figures S2–S4, Data S2 and S3, and Table S1.

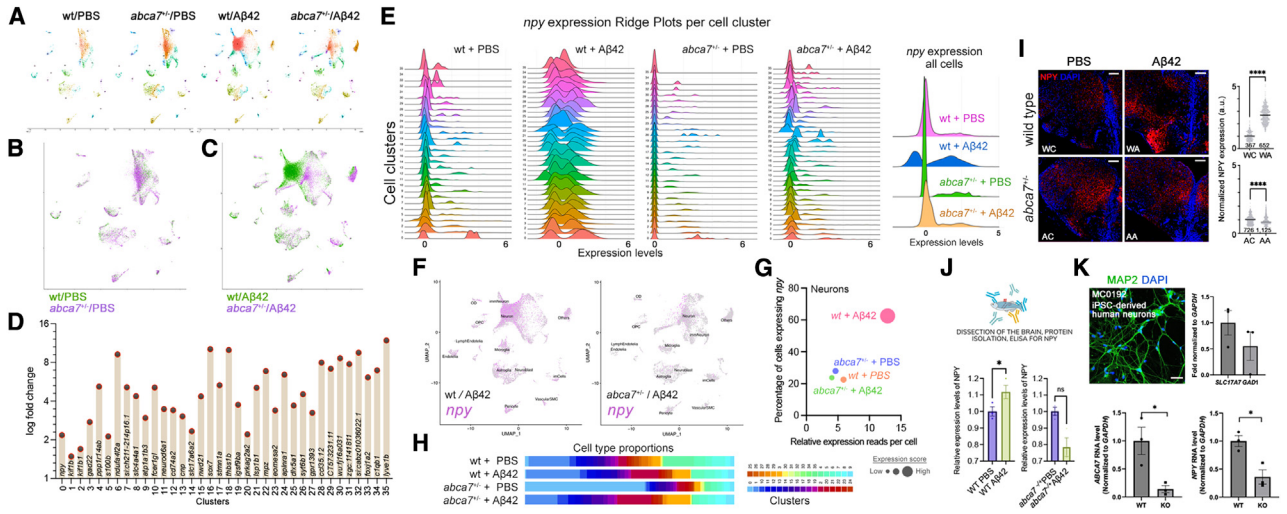

Figure 3. *npy* expression is reduced with *abca7* knockout

(A) UMAP clustering for individual experimental groups of wild-type/PBS, wild-type/Aβ42, *abca7*$^{+/-}$/PBS, and *abca7*$^{+/-}$/Aβ42.

(B) Combined UMAP for wild type (green) and *abca7* knockout (violet) shows overlapping cell clusters.

(C) Combined UMAP for wild-type + Aβ42 (green) and *abca7*$^{+/-}$ + Aβ42 (violet) identifies a specific neuronal cluster (Cluster 0) that is enriched in Aβ42-treated wild-type animals, but this cluster is significantly diminished in *abca7* knockout.

(D) Top marker genes for every cell cluster identify neuropeptide Y (*npy*) as the top marker for cluster 0. Log fold change is a measure of the difference of expression of the top markers in their clusters.

(E) Ridge plots for *npy* expression in wild-type + PBS, wild-type + Aβ42, *abca7*$^{+/-}$ + PBS, and *abca7*$^{+/-}$ + Aβ42 groups in all cell clusters. The rightmost plot is combination of all cells.

(F) Individual expression plots for *npy* in wild type (left) and *abca7* knockout (right) after Aβ42. Cluster 0, expressing *npy*, is strongly reduced.

(G) A Distribution graph for expression score of *npy* in neurons. Expression score is a combinatorial measure for the percentage of cells expressing *npy* (y axis) and the average relative read number per cell (x axis). Amyloid induces the expression score in wild-type animals but not in *abca7* knockout.

(H) Proportions of all cell clusters in wild-type and *abca7*$^{+/-}$ animals with and without Aβ42.

(I) Immunofluorescence for Npy with DAPI counterstain in wild-type and *abca7* knockout animals with or without amyloid toxicity (WC, wild-type + PBS control; WA, wild-type + Aβ42; AC, *abca7*$^{+/-}$ + PBS control; AA, *abca7*$^{+/-}$ + Aβ42). Quantification of image fluorescence intensities shown in the graph. One-way ANOVA with Brown-Forsythe and Welch post test with two-stage linear step-up procedure of Benjamini, Krieger, and Yekutieli correction was used for statistical analyses.

(J) ELISA assay for Npy. Aβ42 induces Npy protein in wild-type animals but not in *abca7* knockout. Parametric t test was used for statistical analyses.

(K) MAP2 immunostaining and RT-qPCR for excitatory (*SLC17A7*) and inhibitory (*GAD1*) neuron markers. Lower graphs show RT-qPCR results for the expression of *ABCA7* and *NPY* in control and *ABCA7* knockout neurons.

Data points are technical replicates. *$p < 0.05$, ****$p < 0.0001$; not significant (ns), $p > 0.05$. Scale bars, 50 μm. See also Figures S2–S4; Data S1, S2, and S3; Table S1.

altered. In ODs, differentially expressed genes (DEGs) enriched lipid metabolism and lipoprotein activity-related processes, as shown previously.[44,46,57] These results suggested that ABCA7 function is related to NPY signaling. The data indicate a previously unidentified regulatory role of ABCA7 on astroglial activity. This appears to connect Aβ42-induced astroglial proliferation with regenerative neurogenesis, a phenomenon relevant to synaptic integrity.[9–11,15,27,30] Further elucidation of these mechanisms may reveal why such regenerative neurogenesis response is not seen in mammalian models.[24,25,28,33,58,59]

To determine how the gene expression in every cell cluster in the individual experimental and control groups change with respect to Aβ42 and *abca7* knockout, we generated the UMAP plots for four groups: wild type/PBS, *abca7*$^{+/-}$/PBS, wild type/Aβ42, and *abca7*$^{+/-}$/Aβ42 (Figures 3A–3C and S2A). Although all cell clusters contained sequenced cells, neuronal cluster 0 was significantly more abundant in only wild-type/Aβ42-injected samples (green in Figure 3C), compared to *abca7*$^{+/-}$/Aβ42 cells (violet in Figure 3C). This cluster was also present in control vehicle PBS-injected wild-type and *abca7*$^{+/-}$ samples (Figure 3B), suggesting that Aβ42-injection might be inducing a specific set of neuronal mechanisms, reversible by *abca7* knockout. To determine the marker genes of every cell cluster, we plotted the expression level of the top expressed gene per cluster (Figure 3D and Data S3) and found that neuropeptide Y (*npy*) was the most expressed gene in Aβ42-related neuronal cluster 0. By plotting the expression levels of *npy* per cell cluster in ridge plots (Figure 3E), we found that *npy* expression was significantly increased in many cell types upon Aβ42 injection (Figure 3E, plots for wild type + PBS and wild type + Aβ42), while *abca7*$^{+/-}$ knockout abrogated this response (Figure 3E, plots for *abca7*$^{+/-}$ + PBS and *abca7*$^{+/-}$ + Aβ42). This is also true when all cells are considered together (Figure 3E, plot for *npy* expression in all cells). Expression of *npy* after Aβ42 in wild-type and *abca7*$^{+/-}$ knockout animals (Figure 3F) is most affected in neurons, as the induction of *npy* after Aβ42 is abrogated with loss of *abca7* function (Figure 3G). Determination of the cell proportions of the individual clusters showed the most pronounced

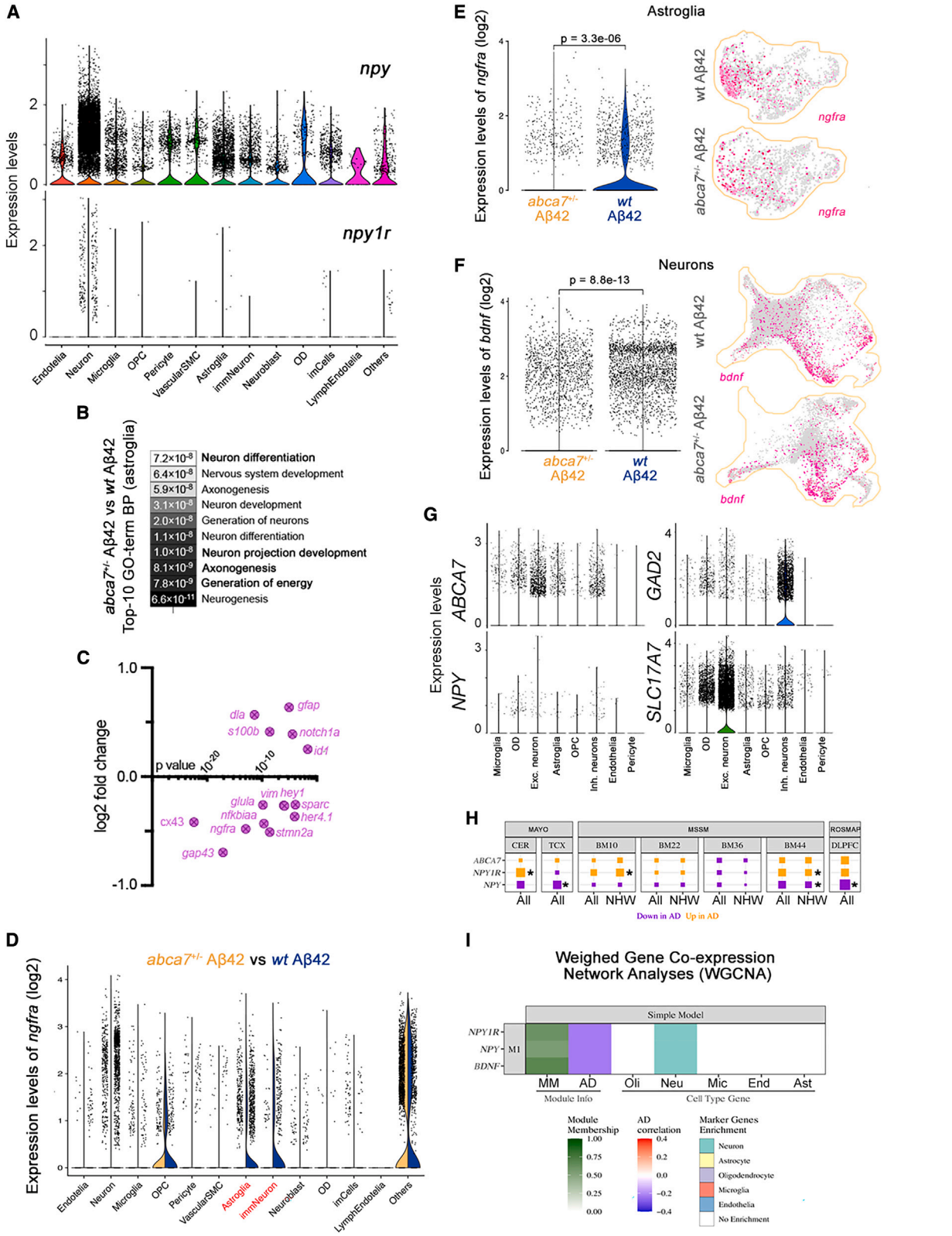

(legend on next page)

alteration in cluster 0, confirming our results (Figures 3H and S2D).

Immunostainings for NPY confirmed the expression of the protein in the telencephalon (Figure 3I). We validated the *abca7*-dependent induction of *npy* gene expression at the protein level with fluorescence-based image quantifications (Figure 3I and Data S1) and with ELISA analyses from brain lysates (Figure 3J and Data S1). In both analyses, Aβ42 induced NPY protein levels in wild-type animals but not in *abca7*$^{+/-}$ knockout animals (Figures 3I and 3J). We verified these findings with cross-species comparison in human neurons generated from patient-derived iPSCs (MC0192), which were extensively characterized previously for their pluripotency, differentiation into neurons, electrophysiological activity, isogenicity, and lack of off-target modifications in the genome.[49] We confirmed the differentiation of these iPSCs into neurons by performing immunostaining with mature neuronal marker MAP2 and RT-qPCR for inhibitory and excitatory neurons, *GAD1* and *SLC17A7*, respectively (Figure 3K). We found that with *ABCA7* knockout in iPSC-derived neurons, *NPY* expression is reduced (Figure 3K), confirming that Aβ42-induced *NPY* expression requires *ABCA7* function.

Npy is required for neurogenesis and synaptic integrity

To predict the target cells of *npy*, we determined the expression of neuropeptide receptors (Figure S2E). Among the most highly expressed NPY receptors was *npy1r*, and its expression was predominantly in neurons (Figures 4A and S2E), Since we observed a change in astroglia proliferation with *abca7* knockout after Aβ42 injection (Figure 1), we hypothesized that NPY signaling could influence astroglia. When we compared the most enriched ten GO terms in astroglia between *abca7*$^{+/-}$/Aβ42 and wild type/Aβ42, we found a significant enrichment in neurogenesis and neuronal differentiation programs (Figure 4B). The differentially expressed genes in the top ten GO terms included upregulated quiescence-related genes *id1*, *dla*, and *notch1a*, as well as gliosis-related genes *s100b* and *gfap*, while several genes related to neurogenic potential and proliferation such as *her4.1*, *stmn2a*, *sparc*, and *hey1* were downregulated (Figure 4C). Interestingly, we also determined a downregulation in *ngfra*, which we have previously shown to be a key regulator of Aβ42-dependent astroglial proliferation and neurogenesis in adult zebrafish brain[9,10] and sufficient to induce proliferation and neurogenesis from otherwise non-neurogenic astroglia in APP/PS1dE9 mouse model of AD.[30] When we detected the *ngfra* expression in individual cell types in comparison of *abca7*$^{+/-}$/Aβ42 to wild type/Aβ42, we found that *ngfra* expression was significantly reduced in astroglia and immature neurons (Figures 4D and 4E), suggesting that *abca7*-dependent regulation of astroglial proliferation could be via *ngfra*, a determinant of neurogenic potential of astroglia.[10,30] We previously showed that brain-derived neurotrophic factor (BDNF) is an intermediate for the neuro-glial crosstalk for regulation of astroglia proliferation,[10] and in this study we found that *bdnf* expression overlaps with *npy* expression in zebrafish brain (Figure S3A). Therefore, we hypothesized that the *npy*-expressing neurons and *ngfra*-expressing astroglia could be communicating through BDNF. To test this, we determined the *bdnf* expression and changes in our dataset. We found that *bdnf* expression was significantly reduced in neurons of *abca7*$^{+/-}$/Aβ42 groups in comparison to the wild-type/Aβ42 group (Figure 4F), suggesting that alterations in astroglial proliferation and neurogenic potential in *abca7*$^{+/-}$ animals could be due to reduced *bdnf* in neurons and reduced *ngfra* in astroglia. Our findings suggest that ABCA7 influences astroglial proliferation through a previously unidentified pathway linked to NPY signaling. Given the ubiquitous nature of dysregulated NPY signaling across various cell types in AD, the specificity of this mechanism to astroglia in zebrafish presents an intriguing avenue for research.

The NPY-BDNF-NGFR axis is associated with Alzheimer's disease

While brains in zebrafish and humans are evolutionarily distinct, pathological mechanisms of AD are comparable,[6,8–10,16,17,20–22,24–26,30,32,33,58,61,62] exemplified by the remarkable similarity of molecular changes in neurons after amyloid toxicity.[58] Thus, we hypothesized that NPY and BDNF signaling might be altered in AD patients. To test this, we first determined the expression of *ABCA7* and *NPY* in single nuclei transcriptomics study of human brains[19,60,63] and found that *ABCA7* and *NPY* were expressed in inhibitory and excitatory neurons, while *ABCA7* expression was also present in microglia and oligodendrocytes (Figure 4G and Data S4). We analyzed human bulk RNA sequencing (RNA-seq) in brain tissue from the Mayo Clinic, ROSMAP, and Mount Sinai Brain Bank (MSBB). In cerebellum (CER) and superior temporal gyrus (TCX) regions,[64,65] Brodmann areas BM10, BM22, BM36, and BM44 brain regions,[66] and dorsolateral prefrontal cortex (DLPFC),[67] we found that *NPY* had a consistent downregulation trend in all cohorts (significantly downregulated in AD in Mayo-TCX, ROSMAP, and MSBB BM44; $p < 0.05$; Data S5 and

Figure 4. NPY is reduced in Alzheimer's brains and interacts with BDNF-NGFR signaling

(A) Violin plot for *npy* and *npy1r* expression in every identified cell type in zebrafish.

(B) Top ten enriched GO terms when *abca7*$^{+/-}$ + Aβ42 and wild-type + Aβ42 were compared indicate altered neurogenesis mechanisms in astroglia.

(C) Neurogenic genes are downregulated and quiescence genes are upregulated in astroglia after *abca7* knockout.

(D) Violin plot for expression of *ngfra* in astroglia when *abca7*$^{+/-}$ + Aβ42 is compared to wild-type + Aβ42.

(E) Expression of *ngfra* is strongly reduced in astroglia.

(F) Ngfra ligand Bdnf is significantly reduced in neurons.

(G) Expression of *ABCA7* and *NPY* in human brains (data reanalyzed from Lau et al.[60]), showing co-expression in neurons.

(H) Expression analyses in various AMP-AD brain transcriptome datasets indicate uniform downregulation of *NPY* with AD. Asterisks indicate statistical significance ($p < 0.05$).

(I) Weighed gene co-expression network analyses based on Mayo Clinic temporal cortex (TCX) RNA-seq data indicate *NPY*, *NPY1R*, and *BDNF* expressions are negatively correlating with AD and are associated with neurons.

See also Figure S4; Data S1, S2, S3, S4, and S5; Tables S1–S3.

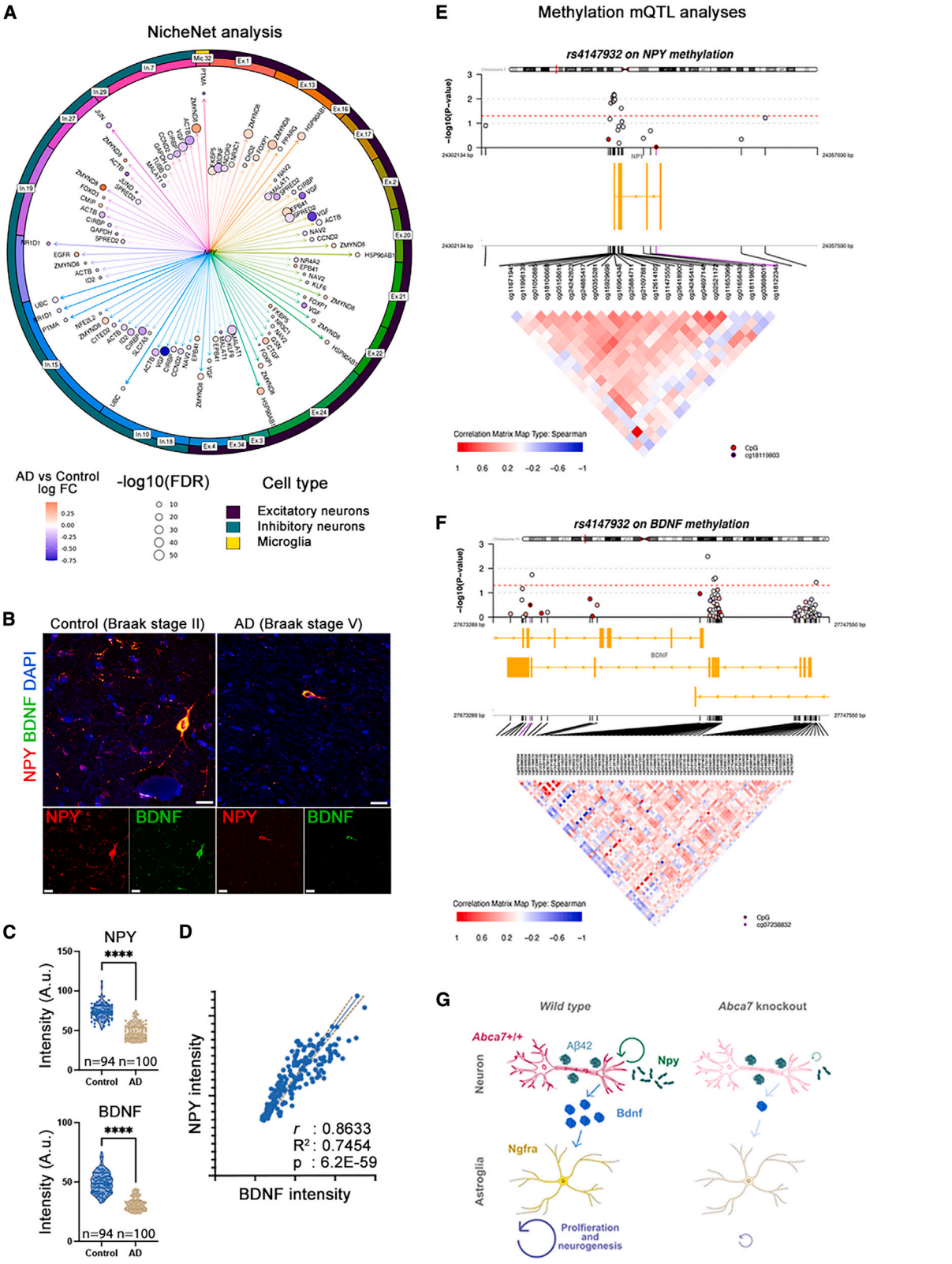

(legend on next page)

Table S2). NPY receptor *NPY1R* is upregulated in Mayo-CER and MSBB BM10 and BM44 ($p < 0.05$; Figure 4H and Data S4). In Mayo-CER and Mayo-TCX, *BDNF* is significantly downregulated in AD in (FDR = 0.015 and 2.1E−6, respectively; Data S4). To determine whether bulk RNA-seq results are consistent with comprehensive single-nucleus datasets in AD patients, we analyzed a recent extensive single-cell atlas across 427 individuals and 2.3 million brain cells, whereby a differential expression analysis at the level of specific cell types and across different stages of disease progression defined by global AD pathology scores was conducted.[68] Consistent with our findings, *NPY* expression was significantly downregulated in inhibitory neurons at the early stages of the disease (log fold change −0.547, $p = 7.4E-03$; https://github.com/mathyslab7/ROSMAP_snRNAseq_PFC), suggesting that reduced *NPY* expression is an early event in disease pathology. Additionally, the consistency between bulk and single-cell RNA results and the normalized read number analyses performed in different AD cohorts indicate that the reduction in *NPY* levels is not a confounding consequence of neuronal loss but a specific feature of disease etiology.

To determine whether *NPY* and *NPY1R* were associated with AD through co-expression modules of gene expression, we performed weighted gene co-expression network analysis (WGCNA) on the Mayo-TCX brain samples and found that this module was significantly downregulated in AD and enriched with neuronal genes (Figure 4I). Through NicheNet[69] analysis, which predicts the cellular interactions through candidate ligand-receptor pairs, we found that in humans, *NPY* interacted with several cell types to regulate the expression of various genes in target cells (Figure 5A and Data S4). The hits include *BDNF* in excitatory neurons, *SLC7A5* in inhibitory neurons, and *AGT* in astrocytes (Data S5). Interestingly, in the largest excitatory neuron cluster, the highest gene-expression change was observed in *BDNF* (Figure 5A), suggesting that the NPY-BDNF-NGFR axis was similar in humans and zebrafish. When we compared the NicheNet targets in humans (Figure 5A) to our previous dataset in the mouse model of AD where the molecular regulation of induced nerve growth factor receptor (NGFR) signaling was analyzed,[30] we found that 52.8% (19/36) of the genes that were potential NPY targets in humans (Figure 5A) were also differentially regulated after *NGFR* expression in the hippocampus of the APP/PS1 mouse model of AD (Figure S3B). This finding suggested potential crosstalk mechanisms between NPY-expressing neurons and NGFR-expressing astroglia via BDNF. We confirmed this interaction by immunostaining in postmortem human brains (controls vs. AD) coupled to image quantifications (Figures 5B and 5C) and found that in AD brains, NPY and BDNF co-localize in neurons, and their levels were reduced in AD compared to controls (Figures 5B and 5C; Data S1). NPY and BDNF levels in the brain significantly correlated in neurons ($R^2 = 0.74$, $p = 6.2E-59$; Figure 5D).

Loss-of-function variants in *ABCA7*, *NGFR*, and *BDNF* segregate in AD families

Our findings propose that *ABCA7*-dependent NPY activity could establish a neuro-glial crosstalk through BDNF and NGFR that regulates astroglial physiology, and genetic variants in these genes may be associated with familial AD. Results from family-based studies (demographics in AD-FBS (AD Family-Based Study) and EFIGA (Estudio Familiar de Influencia Genetica en Alzheimer) comprising Hispanics and non-Hispanic whites: Table S3) showed that the *ABCA7* gene was completely (Table S3) and incompletely (Table S4) segregating in both cohort families. Two variants from the *ABCA7* genes were segregating in the Hispanic and two variants were segregating in the white non-Hispanic AD families (Table S4). This indicates the strong association of *ABCA7* with familial AD. Additionally, a frameshift variant in the *BDNF* gene was completely segregating (Tables S3 and S4) in the white non-Hispanic families but not segregating in the Hispanic families. In the *BDNF* gene, a frameshift variant was segregated in white non-Hispanic families but co-segregated with *APOEε4* (Table S4). Taken together, the *ABCA7-NPY-BDNF-NGFR* axis appears relevant to familial AD and likely more pronounced in the white non-Hispanic ancestry. These results also suggest that NPY activity may run through the downstream BDNF and NGFR signaling axis.

ABCA7, *NPY*, and *NGFR* co-expression is associated with higher Braak staging in human brains

As *NPY* expression was reduced in AD (Figure 4, Table S2, and Data S5), we investigated whether Braak stages were also associated with co-expression among our five genes (*ABCA7*, *BDNF*, *NPY*, *NPY1R*, and *NGFR*), adjusting for sex, age at death, RNA integrity number, and race (Table S5). Indeed, our data confirmed that two statistical interactions were significant after multiple testing correction: *NPY*NGFR* (odds ratio

Figure 5. NPY interacts with BDNF-NGFR signaling

(A) *NPY*-centered NicheNet analysis in human brain datasets of single-nucleus RNA-seq. Excitatory neurons cluster 1 showed reduced *BDNF* in AD in an *NPY*-dependent manner. Arrows represent the cumulative measure for log fold change.

(B) Double immunohistochemistry for NPY and BDNF in postmortem control and AD brains. Scale bars, 10 μm.

(C) Quantification results of NPY and BDNF intensities in neurons. Two postmortem brains used per group. *n* denotes the number of neurons analyzed. Asterisks denote $p < 1.0E-15$ (non-parametric Kolmogorov-Smirnov test).

(D) Correlation analyses between BDNF and NPY in 194 neurons analyzed (simple linear regression).

(E and F) CpG methylation mQTL analyses with *ABCA7* variants in humans. The epigenetic changes on *NPY* (E) and *BDNF* (F) are shown. Red line indicates statistical significance cutoff. Every circle represents one methylation site. Blue indicates hypermethylation, and red indicates hypomethylation. Yellow bars indicate the gene location and coding direction. Enlarged region lists all methylation sites in the corresponding genomics window. Correlation matrices between different methylation sites are depicted as positive (red) and negative (blue). *ABCA7* variants exert methylation changes in *NPY* and *BDNF* promoters in a highly correlated manner.

(G) Working model for Abca7-dependent Npy activity.

****$p < 0.0001$. See also Figure S4; Data S1, S2, S3, S4, and S5; Tables S1–S3.

[OR] = 2.06 [1.28–3.70]) and *ABCA7*NGFR* (OR = 3.29 [1.48–8.72]), consistent with our previous hypothesis that the *ABCA7-NPY* axis can act through *NGFR* signaling and that this interaction might be associated with increasing Braak stages in AD. By depicting co-expression patterns of *ABCA7*, *NPY*, and *NGFR*, we found that *NGFR* expression inversely correlates with *ABCA7* and *NPY* expression only when AD pathology is absent or mild (Braak 0–4), while in AD pathology (Braak 5–6), this correlation was lost (Figure S3C). These results suggest that in mild cases or controls, reduced *ABCA7* or *NPY* leads to an increase in *NGFR* as a potential protective reaction, which can be absent in AD; when *NPY* and *ABCA7* expression is reduced, AD brains cannot elevate *NGFR* levels. This statistically significant differential interaction dependent on the Braak stage was consistent with our previous study in which activation of *NGFR* in the brains of APP/PS1dE9 mice reduced amyloid and Tau burden.[30]

ABCA7 variants are associated with epigenetic regulation of *NPY*, *BDNF*, and *NGFR*

To further test the potential regulatory role of *ABCA7* on *NPY*, *BDNF*, and *NGFR*, we identified potential methylation quantitative trait locus (mQTL) signals of *ABCA7* variants in humans using New York Brain Bank and NIA AD-FBS/NCRAD cohorts[70,71] (Figures 5E and 5F). According to the regional plots (Figures 5E and 5F), we observed that the genetic variants at *ABCA7* have nominally significant mQTL effects ($p < 0.05$) on the methylation at loci of *ABCA7*, *NPY*, *BDNF*, and *NGFR* at transcriptional regulatory regions (Figures 5E and 5F; Data S5). This indicated that *ABCA7* might influence the expression of *NPY*, *BDNF*, and *NGFR* through epigenetic regulation and potentially through transcriptional activity.

BDNF and NGFR signal axis mediates ABCA7-dependent NPY activity

Considering our previous results (Figures 1, 2, 3, and 4), we hypothesized that *abca7*-expressing neurons could induce *npy* after Aβ42, which could run through the *npy* receptor to allow production of BDNF that regulates astroglial proliferation in zebrafish via NGFR (Figure 5G). This cascade could be impaired by *abca7* knockout through reducing *npy* availability, *bdnf* expression, NGFR signaling, in turn modulating the synaptic integrity and astroglial proliferation. To test this hypothesis, we injected human NPY alone or together with Aβ42 to *abca7*$^{+/-}$ knockout zebrafish and compared these to PBS- and Aβ42-injected groups (Figure 6A) to investigate whether NPY could ameliorate the alterations in astroglial proliferation, synaptic degeneration, and microglial activity. By performing immunostaining for synaptic vesicle protein SV2 as a neuronal marker and L-plastin as a microglial marker (Figure 6B), and GS as an astroglial marker and PCNA as a proliferating cell marker (Figure 6B), we found that NPY was sufficient to counteract the reduction of SV2-positive synaptic puncta in Aβ42-treated *abca7*$^{+/-}$ neurons and increase the astroglial proliferation while not affecting the number of microglial cells (Figures 6C and S1B; Data S1).

Since BDNF expression is affected by ABCA7 in zebrafish and humans (Figure 4), we hypothesized that ectopic NPY could also rescue the expression of BDNF in *abca7* knockout animals. Through immunostaining of BDNF and image quantifications, we determined that *abca7* knockout hampered the induction levels of BDNF after Aβ42 in comparison to wild-type animals, while NPY can rescue the normal BDNF levels after Aβ42 even in the *abca7* knockout background (Figure 6D). This indicates that NPY acts upstream of BDNF. Since ectopic NPY rescued the reduced synaptic integrity in *abca7*$^{+/-}$ animals (Figure 6C) and increased BDNF expression (Figure 6D), we hypothesized that BDNF could also increase the synaptic integrity in *abca7*$^{+/-}$ animals after Aβ42. We found that ectopic BDNF increased SV2-positive puncta in *abca7*$^{+/-}$ knockouts (Figure 6E) without altering the number of microglia, consistent with the results of ectopic NPY (Figures 6C and 6E). These results suggest that ABCA7-dependent NPY and BDNF act in concert to maintain synaptic integrity after amyloid toxicity.

Since we previously showed that NGFR signaling, which is also reduced in AD (Figures 4 and S3C), is downstream of BDNF,[10,30] we hypothesized that the synaptoprotective effects of NPY and BDNF could run through NGFR signaling. To test this, we inhibited NGFR by using a selective blocker that effectively reduces downstream NGFR signaling in nuclear factor κB reporter zebrafish (Figure S3D). We found that ectopic co-treatment of BDNF and NGFR inhibitor effectively reduced the BDNF-induced SV2-positive puncta and PCNA-GS double-positive proliferating astroglia in the *abca7*$^{+/-}$ background (Figures 7A and 7B), indicating that BDNF signaling acts through NGFR. The microglial numbers are not affected by NGFR inhibition after BDNF, indicating that a mechanism independent of the NPY-BDNF-NGFR signaling axis governs microglial activity in *abca7*$^{+/-}$ knockout, consistent with our previous findings (Figures 1 and 6C). Finally, we validated our findings through an independent *npy*$^{-/-}$ knockout zebrafish model in which *npy* loss of function reduced SV2-positive synaptic puncta and BDNF expression (Figures 7C and 7D). Overall, these results show that ABCA7-dependent NPY signaling is required for inducing a BDNF/NGFR signaling axis that maintains synaptic integrity and astroglial proliferation, which are required for brain resilience to AD (Figure 7E).

DISCUSSION

In this study, we generated the first stable adult *abca7* gene knockout in zebrafish and investigated the impact of heterozygous *abca7* deletion in zebrafish brains in the presence and absence of amyloid toxicity. The *abca7*$^{+/-}$ zebrafish exhibited altered responses to Aβ42 toxicity, with reduced astroglial proliferation and synaptic density. *npy* levels increased in neurons due to Aβ42 in wild-type zebrafish but decreased with *abca7*$^{+/-}$ knockout, potentially abrogating a beneficial response in neurons. Injecting human NPY restored altered processes and BDNF expression in *abca7*$^{+/-}$ zebrafish. BDNF can recapitulate this rescue, and NPY-induced BDNF acts through NGFR as blockage of NGFR suppressed the effects of BDNF. Comparative studies validated the changes in *NPY* expression in human AD brains and its regulatory signaling through *BDNF*. In human iPSCs, *ABCA7* knockout also reduces *NPY* expression. Our results uncovered a potential role of *ABCA7* as a synaptic resilience and neurogenic factor.

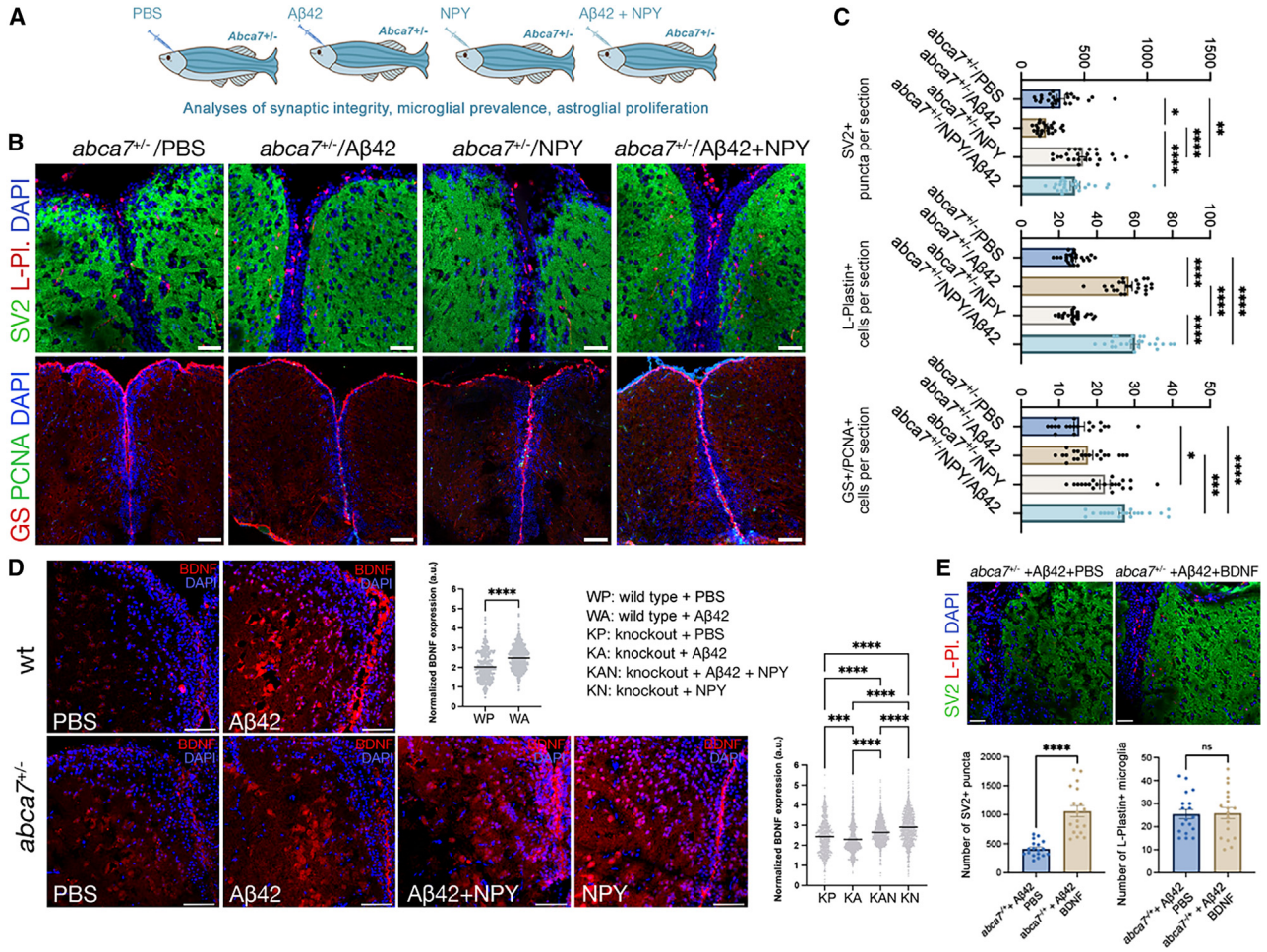

Figure 6. ABCA7 regulates synaptic integrity and astroglial proliferation through BDNF

(A) Experimental setup for investigating the biological relevance of NPY to *abca7* function and amyloid-induced alterations in synaptic integrity, microglial activity, and astroglial proliferation.

(B) Immunofluorescence for SV2 + L-plastin and GS + PCNA with DAPI counterstains in *abca7*$^{+/-}$ + PBS, *abca7*$^{+/-}$ + Aβ42, *abca7*$^{+/-}$ + NPY, and *abca7*$^{+/-}$ + Aβ42 + NPY brains.

(C) Quantification for number of SV2-positive synaptic puncta, L-plastin-positive microglia, and GS/PCNA double-positive proliferating astroglia. $n = 4$ animals from both sexes and ≥20 brain sections per group. One-way ANOVA with Tukey's multiple comparison test was used for statistical analyses. No comparison bar indicates no significance.

(D) BDNF immunoreactivity in wild-type and *abca7* knockout zebrafish with and without Aβ42. Aβ42 induced BDNF (red) in wild-type animals but not in *abca7* knockout. Injection of NPY with or without Aβ42 restores the induced BDNF expression levels. Non-parametric Kolmogorov-Smirnov test comparing cumulative distributions and one-way ANOVA with Tukey's multiple comparison test were used for statistical analyses.

(E) Immunofluorescence for SV2 and L-plastin with DAPI counterstain in *abca7*$^{+/-}$ + Aβ42 + PBS and *abca7*$^{+/-}$ + Aβ42 + BDNF zebrafish brains. Quantification for the number of SV2-positive synaptic puncta and the number of L-plastin-positive microglia. Non-parametric Kolmogorov-Smirnov test comparing cumulative distributions was used for statistical analyses.

BDNF rescues synaptic integrity changes in *abca7*$^{+/-}$ knockout similar to NPY. $n = 4$ animals from both sexes, with 18 brain sections per group. $^{*}p < 0.0332$, $^{**}p < 0.0021$, $^{***}p < 0.0002$, $^{****}p < 0.0001$; not significant (ns), $p > 0.0332$. Scale bars, 50 μm. See also Figures S1 and S4, Data S1 and S3, and Table S1.

This study confirms and augments the role of *ABCA7* in multiple cellular mechanisms including neuronal response to amyloid, immune system activity, and astroglial proliferation through involvement of NPY, a 36-amino-acid peptide with neuroprotective effects and anti-inflammatory roles.[72–80] Among the highest expression of *NPY* in human brain is in hippocampus,[81–83] the primary neurogenic location. *NPY* expression was reduced in AD in humans[72,82,84,85] and animal models,[77,78] which indicated a protective and beneficial effect of this gene for the homeostatic health of the brain. A recent large single-nucleus transcriptomics study in human brains also confirms our findings. This study identified that *NPY*- and *SST*-expressing inhibitory neurons reduce *NPY* expression in AD and suggested that such alterations could constitute a mechanism that impairs brain resilience with aging and AD.[68] Our study also identified *NPY* and *SST* to be co-expressed in inhibitory neurons (Figure S3E), and *NPY*

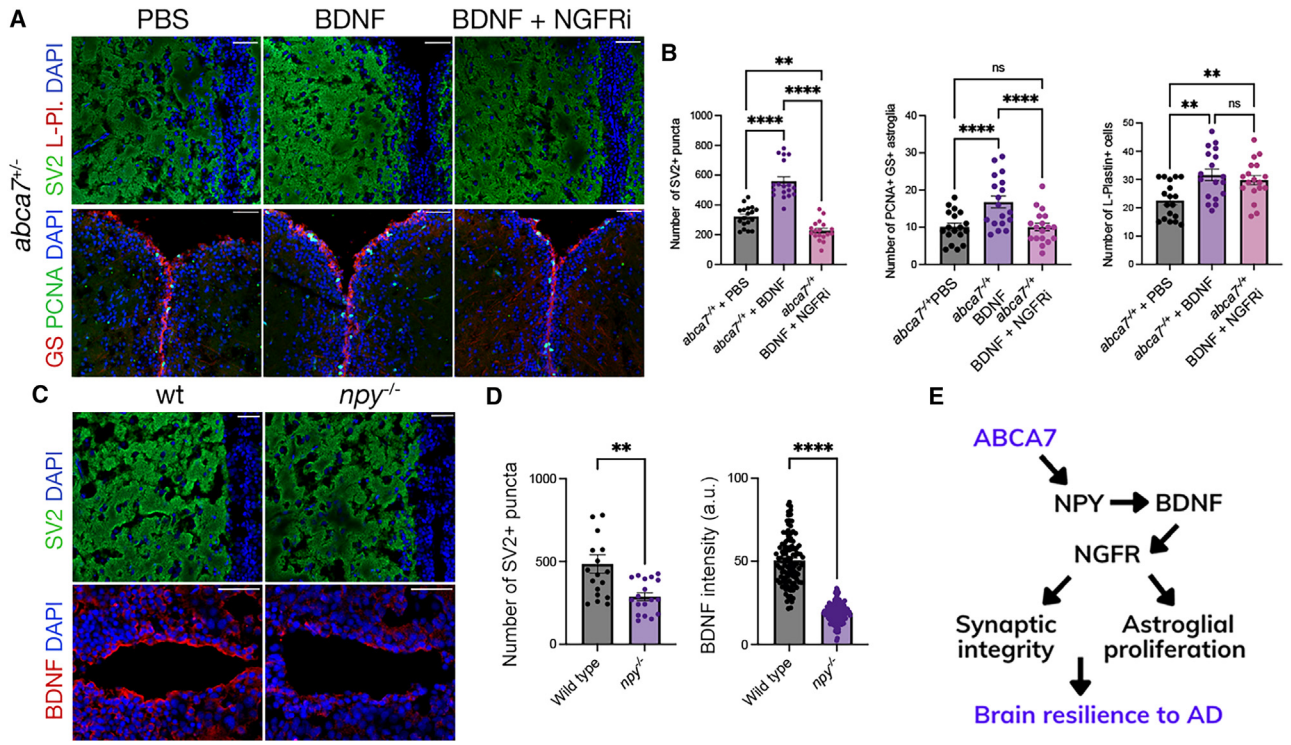

Figure 7. ABCA7-dependent NPY acts through BDNF/NGFR axis

(A) Immunofluorescence for SV2/L-plastin and GS/PCNA with DAPI counterstain in *abca7*$^{+/-}$ knockout brains injected with vehicle (PBS), BDNF, and BDNF + NGFR inhibitor.

(B) Quantification graphs for SV2^{+} puncta, number of PCNA/GS double-positive astroglia, and number of L-plastin^{+} microglia. Inhibition of NGFR abrogates the rescue effects of BDNF on synaptic integrity and astroglial proliferation. Two-way ANOVA with Tukey's multiple comparison test was used for statistical analyses. n = 4 animals from both sexes, with 18 brain sections per group.

(C) Immunofluorescence in *npy*$^{-/-}$ knockout animals for SV2 and BDNF with DAPI nuclear counterstain.

(D) Quantification of the number of SV2+ synaptic puncta and BDNF intensity. *npy*$^{-/-}$ knockout independently reduces BDNF expression and the synaptic integrity. n = 3 animals from both sexes and 18 brain sections per group.

(E) Activity model for ABCA7: ABCA7-dependent induction of NPY after amyloid toxicity is required for expression of BDNF, which—through NGFR—regulates the synaptic integrity and astroglial proliferation. ABCA7 function is relevant to brain resilience to AD in an NPY-dependent manner.

*p < 0.0332, **p < 0.0021, ***p < 0.0002, ****p < 0.0001; not significant (ns), p > 0.0332. Scale bars, 50 μm. See also Figures S1 and S4, Data S1 and S3, and Table S1.

decreased in AD in association with Braak staging. We add further mechanistic insight into the role of NPY-expressing neurons in brain resilience against AD and propose that this mechanism is *ABCA7* dependent. Our transcriptomics and functional studies suggest that NPY might be related to sustained neurotrophic effect through regulation of the availability of BDNF. Our NicheNet analyses supported the notion that the change in NPY in human brains was linked to reduced BDNF in neurons in human brains (Figure 5). These findings were consistent with the previous observations that Npy positively regulates *Bdnf* expression in rat cortical neurons exposed to Aβ42.[76]

We also found that the *abca7* knockout reduced the proliferation of astroglia, which was consistent with the reduced expression of *ngfra*, a key regulator of astroglial proliferation and neurogenesis in zebrafish brain after amyloid toxicity. Astroglia, as neural stem cells (NSCs), could inform regenerative therapies.[59,86–91] The use of endogenous NSCs may limit tissue loss and improve tissue integrity, with potential therapeutic applications in neurodegeneration.[28,92] Thus, a promising strategy could involve stimulating endogenous astroglia to produce new neurons, thereby replacing the lost ones and enhancing the brain's resilience to neurodegeneration. Previous studies showed that induced *in vivo* expression of *Npy* in a mouse model of AD can increase neural progenitor cell proliferation and neurogenesis.[74] We found that *abca7* significantly reduced amyloid-induced *npy* expression, the reduction of which reduces the proliferative response of astroglia. This reduction can be rescued by human NPY or BDNF independently.

Taken together, we propose that ABCA7 is required for increased NPY as a response to AD-related neuropathology and that NPY activity is crucial for synaptic integrity and astroglial proliferation in AD. These two processes may help to maintain homeostatic brain resilience, which might be impaired in AD. This hypothesis is supported by our genetic association studies in which *ABCA7* and *NPY* expression is associated with *NGFR* in low-Braak stages of AD but not in high-Braak stages (Figure S3C). In conjunction with our previous findings that NGFR imposes proliferative and neuroregenerative potential to the

astroglia of APP/PS1dE9 AD mouse model and reduces the amyloid and Tau burden,[30] these results support the notion that the protective role of NGFR signaling in mammalian brains against AD is impaired with advancing AD pathology. In AD brains, reduction in *NPY* expression was present in all regions but prominently in the hippocampal region, suggesting that *NPY* signaling could regulate neurogenesis. The hippocampus, one of the first brain regions to be affected in AD, contains neural progenitor cells that continue to generate new neurons for the course of adult hippocampal neurogenesis,[25,27,28,93] which is impaired in AD.[94,95] Blocking neurogenesis exacerbates neuronal loss and cognitive decline, while neurogenesis in combination with BDNF treatment ameliorates the behavioral readouts.[96] Therefore, neurogenesis together with neurotrophic mechanisms can sustain the resilience of the brain and the ability to cope with neurodegeneration. Our results suggest that *abca7*, through regulating both neurogenesis and neurotrophic factor expression, may be necessary for protection or resilience against AD neuropathology, also consistent with AD risk associated with both common and rare *ABCA7* genetic variants. Our results propose a previously unknown biological crosstalk between *ABCA7*, *NPY*, *BDNF*, and *NGFR*, which are genetically associated with AD.[5]

While our study primarily focuses on astroglia and neuronal responses, we acknowledge the significant NPY signature observed in other cell types. The emphasis on astroglia and neurons arises from our data, which highlighted these cells' pivotal role in response to Aβ42 toxicity in the context of *abca7* deletion. Notably, neurons showed the most significant upregulation of NPY expression upon Aβ42, a finding that was not observed in the *abca7* knockout, suggesting a critical neuronal response that could be mediated through NPY signaling (Figures 3F and 3G). The astroglial population demonstrated a pronounced downregulation in neurogenic genes and upregulation in quiescence genes after *abca7* knockout (Figures 4B and 4C), further drawing our attention to these cell types. Nevertheless, the widespread NPY expression changes across multiple cell types suggest a broader regulatory role for *ABCA7*, meriting further investigation beyond the scope of this study.

Although we have established a link between *abca7* and *npy*, and subsequent effects on neural resilience and astroglial proliferation, the cellular mechanisms through which *abca7* loss of function alters *npy* expression requires further investigation. ABCA7's impact on lipid metabolism is believed to influence Aβ processing, potentially leading to the aggregation of Aβ neuritic plaques, a hallmark of AD.[36,51] Moreover, ABCA7's interactions with other proteins involved in lipid metabolism and immune-response regulation further underscore its role in AD pathology, where NPY could partake. A possible mechanism could involve the structural and functional assembly of lipid rafts through ABCA7 activity, as this has been demonstrated in lymphocytes[47] and previously hypothesized as a general regulatory pathway.[97] This is consistent with the proposed role of ABCA7 in regulating lipid metabolism and localization on the cell membrane.[44,46,48] NPY also interacts with the lipid bilayer on the cell surface in a conformation-dependent manner,[98] and altered lipid content and organization could affect the activity of NPY directly or indirectly through its various receptors such as *NPY1R*, which we found to be expressed in neurons in humans and zebrafish. Previous studies demonstrated that NPY and BDNF can stimulate each other's expression in a feedforward loop,[76,78,79] suggesting that loss of *ABCA7* function could impair this neurotrophic signaling by disrupting the lipid-mediated NPY signaling, resulting in reduced BDNF expression in neurons. This downregulation of BDNF might affect astroglial behavior, potentially influencing processes such as proliferation and neurogenesis through NGFR-mediated pathways. This crosstalk highlights the interconnectedness of lipid metabolism, NPY signaling, and BDNF-mediated effects on cellular responses in an *ABCA7*-dependent mechanism and suggests potential therapeutic targets and directions.

Large genomic deletions may alter the regulatory elements within the non-coding regions of the genome. Before determining the target part of *abca7* gene to be deleted in zebrafish, we analyzed the DNA sequence based on the latest zebrafish genome annotation (May 2017, GRCz11/danRer11). We found that CpG islands, GC content, repeating elements, and *cis*-regulatory traces were lower compared to other genomic regions (Figure S3F), suggesting that the deletion itself may cause minimal regulatory burden. Our downstream analyses, normalization steps, and cross-species comparison coupled to statistical considerations also support that the changes we observe in our study are unlikely to be associated with regulatory regions deleted during the knockout generation. We also used *abca7* heterozygous knockout, allowing the other strand to compensate for potential *cis*/*trans* regulations in the genome.

We identified expression of *npyr8a* in zebrafish, which can potentially bind to Npy, yet the functional role of this receptor subtype needs further investigation. Although *Abca7* knockout changes microglial activity and numbers, NPY does not, suggesting that Abca7's role on microglial dynamics is NPY independent and requires further analyses. ABCA7 is a critical regulator of lipid metabolism, and it could regulate secretion of neuropeptides or functional maturation and organization of receptor complexes on the lipid bilayer of the membrane. This potential mechanistic relationship requires further analyses of lipid content of Abca7 knockout animals and can point toward a general alteration in secretory pathways. Further studies should also focus on the potential protective role of *ABCA7* in the context of other neurodegenerative pathologies, given that *ABCA7* variants are also associated with the risk of non-AD neurodegenerative diseases.[37,40]

Limitations of the study

Despite its strengths, this study has limitations. The use of iPSC-derived neurons with *ABCA7* knockout is insightful but limited by the number of replicates and iPSC lines. Increasing biological replicates and incorporating diverse donor iPSCs will enhance robustness. Extended disease models, such as knockout mice, will be informative for and add *in vivo* mammalian animal model data. Longitudinal studies examining the effects of *ABCA7* knockout over time may help in understanding the progression of cellular and molecular changes associated with AD. Finally, the interaction of *ABCA7* knockout with other genetic, epigenetic, and environmental factors that contribute to AD can be explored to provide a more comprehensive view of its role in disease pathogenesis.

RESOURCE AVAILABILITY

Lead contact

Further information and requests for resources and reagents should be directed to and will be fulfilled by the lead contact, Caghan Kizil (ck2893@cumc.columbia.edu).

Materials availability

The knockout zebrafish line is available upon reasonable request.

Data and code availability

Accessible datasets are as follows: NCBI-GEO: GSE244550 (single cell dataset), AD Knowledge Portal: https://adknowledgeportal.synapse.org (bulk brain RNA seq dataset in AMP-AD).

ACKNOWLEDGMENTS

We would like to thank the Taub Institute for Research on Alzheimer's Disease and its Aging Brain Imaging platform and the Molecular Pathology platform of the Columbia University Herbert Irving Comprehensive Cancer Center for help, New York Brain Bank for postmortem human brain sections, Dr. Stanislava Popova for help with gRNA design, Dr. Rajesh K. Soni (Proteomics and Macromolecular Crystallography, Columbia University) for protein extraction, Dr. Bengisu Turgutalp for selection of inhibitors, Erin Bush (JP Sulzberg Genome Center) for sequencing, and Michael Kissner from the Flow Cytometry Core Facility (CCTI, supported in part by the Office of the Director, National Institutes of Health under awards S10OD020056) of the Columbia University Herbert Irving Comprehensive Cancer Center for procedural support. The single-cell sequencing was performed by the Single Cell Analysis Core and Columbia Genome Center at the Sulzberger Genome Center, which was funded in part through the NIH/NCI Cancer Center support grant P30CA013696 and used the Genomics and High-Throughput Screening Shared Resource. Part of the data generation for this publication at Columbia University was also supported in part by the National Center for Advancing Translational Sciences, National Institutes of Health, through grant number UL1TR001873. We thank the contributors who collected samples used in this study. We thank the patients and families for their participation, without whom these studies would not have been possible. This work was supported by Columbia University Schaefer Research Scholar award (C.K.); the Thompson Family Foundation Program for Accelerated Medicines Exploration in Alzheimer's Disease and Related Disorders of The Nervous System (TAME-AD) (C.K.); Taub Institute grants for Emerging Research (TIGER) (C.K.); Toffler Scholar Program (P.B.); National Institute on Aging R01AG067501 (R.M., G.T., B.N.V., and C.K.); National Institute on Aging U24AG056270 (R.M., B.N.V., and C.K.); National Institute on Aging RF1AG066107 (R.M., B.N.V., and C.K.); National Institute on Aging U01AG046139, U19AG074879, and R01AG061796 (N.E.-T.); Alzheimer's Association Zenith awards (N.E.-T.); and FRIPRO research grant from The Research Council of Norway (314189) (N.J.-Y.).

The National Institute on Aging-AD Family-Based Study (NIA AD-FBS; https://www.neurology.columbia.edu/research/research-centers-and-programs/national-institute-aging-alzheimers-disease-family-based-study-nia-ad-fbs) collected the samples used in this study and is supported by National Institute on Aging (NIA) grants U24AG026395, U24AG021886, R01AG041797, and U24AG056270. Additional families were contributed to the NIA-AD FBS through NIH grants R01AG028786, R01AG027944, RO1AG027944, RF1AG054074, and U01AG052410. The NIA-AD FBS began in 2003 with the goal of recruiting large, multiply affected families with late-onset Alzheimer's disease (AD) for genetic research. The study created a resource of well-characterized families with late-onset AD. The initial phases of the Alzheimer's Disease Sequencing Project (ADSP) included genotyping of hundreds of participants from NIA-AD FBS. The ADSP Follow-Up Study heavily engages resources provided by the NIA-AD FBS and depends upon the longitudinal follow-up of families, and the collection of additional families, in particular those from diverse populations. Samples include biological materials for genome-wide association studies and whole-genome sequencing (WGS), peripheral blood mononuclear cells for stem cell modeling, plasma for studies of metabolomics, proteomics, and biomarker research, and brain autopsy materials for bulk RNA-seq.

EFIGA is a study of sporadic and familial AD among Caribbean Hispanics recruited from clinics in the Dominican Republic and New York (R01 AG067501). The goal of this study is to identify genetic variants that increase late-onset AD risk in this ethnic group. This study was initiated in 1998 and recruited individuals and their families in New York as well as from clinics in the Dominican Republic. Recruitment for the EFIGA began in 1998 to study the genetic architecture of AD in the Caribbean Hispanic population. Patients with familial AD were recruited and if a sibling of the proband had dementia, all other living siblings and available relatives underwent evaluation. Cases were defined as any individual meeting NINCDS-ADRDA criteria for probable or possible AD.

The results published here are in whole or in part based on data obtained from the AD Knowledge Portal (https://adknowledgeportal.org). The Mayo RNA-seq study data collection was led by Dr. Nilüfer Ertekin-Taner, Mayo Clinic, Jacksonville, FL, USA as part of the multi-PI U01 AG046139 (MPIs Golde, Ertekin-Taner, Younkin, and Price) using samples from The Mayo Clinic Brain Bank. Data collection was supported through funding by NIA grants P50 AG016574, R01 AG032990, U01 AG046139, R01 AG018023, U01 AG006576, U01 AG006786, R01 AG025711, R01 AG017216, and R01 AG003949; CurePSP Foundation; and the Mayo Foundation. Study data included samples collected through the Sun Health Research Institute Brain and Body Donation Program of Sun City, AZ, USA. The Brain and Body Donation Program is supported by the NINDS (U24 NS072026, National Brain and Tissue Resource for Parkinson's Disease and Related Disorders); the NIA (P30 AG19610, Arizona Alzheimer's Disease Core Center); the Arizona Department of Health Services (contract 211002, Arizona Alzheimer's Research Center); the Arizona Biomedical Research Commission (contracts 4001, 0011, 05-901, and 1001, to the Arizona Parkinson's Disease Consortium); and the Michael J. Fox Foundation for Parkinson's research. Study data were provided by the Rush Alzheimer's Disease Center, Rush University Medical Center, Chicago. Data collection was supported through funding by NIA grants P30AG10161 (ROS), R01AG15819 (ROSMAP; genomics and RNA-seq), R01AG17917 (MAP), R01AG30146, R01AG36042 (5hC methylation, ATAC-seq), RC2AG036547 (H3K9Ac), R01AG36836 (RNA-seq), R01AG48015 (monocyte RNA-seq) RF1AG57473 (single-nucleus RNA-seq), U01AG32984 (genomic and whole-exome sequencing), U01AG46152 (ROSMAP AMP-AD, targeted proteomics), U01AG46161(TMT proteomics), U01AG61356 (WGS, targeted proteomics, ROSMAP AMP-AD), the Illinois Department of Public Health (ROSMAP), and the Translational Genomics Research Institute (genomic). Additional phenotypic data can be requested at www.radc.rush.edu. These data were generated from postmortem brain tissue collected through the Mount Sinai VA Medical Center Brain Bank and were provided by Dr. Eric Schadt from Mount Sinai School of Medicine.

AUTHOR CONTRIBUTIONS

Conceived and designed the study: C.K. Generated the *abca7* knockout line and performed the zebrafish experiments and data analyses: H.T., E.Y., P.B., N.N., N.K., R.M.D., and C.K. Generated the *npy* knockout line: I.Y., J.M.S., and N.J.-Y. Single-cell transcriptomics: E.Y., P.B., M.I.C., and C.K. Postmortem human brains: D.F. and A.F.T. *ABCA7* knockout human iPSCs: N.W. and T.K. Performed human transcriptome and genome data analyses: Y. Min, X.W., Ö.İ., T.I.G., B.N.V., Z.Y., G.T., N.E.-T., and R.M. Analyzed and interpreted the human and zebrafish data: P.B., E.Y., Y. Ma, X.W., Ö.İ, T.I.G., D.R.-D., Z.Y., G.T., B.N.V., N.E.-T., R.M., and C.K. Funding: N.E.-T., R.M., and C.K. Wrote the manuscript: C.K. Revised, edited, and approved the final manuscript: all authors.

DECLARATION OF INTERESTS

C.K. is a co-founder, shareholder, and scientific advisor of Neuron-D GmbH, which had no financial involvement in or influence on this study.

STAR★METHODS

Detailed methods are provided in the online version of this paper and include the following:

- KEY RESOURCES TABLE

SUPPLEMENTAL INFORMATION

Supplemental information can be found online at https://doi.org/10.1016/j.xgen.2024.100642.

Received: December 2, 2023
Revised: May 4, 2024
Accepted: August 8, 2024
Published: August 30, 2024

REFERENCES

1. Reitz, C., Pericak-Vance, M.A., Foroud, T., and Mayeux, R. (2023). A global view of the genetic basis of Alzheimer disease. Nat. Rev. Neurol. *19*, 261–277. https://doi.org/10.1038/s41582-023-00789-z.
2. Dumitrescu, L., Mahoney, E.R., Mukherjee, S., Lee, M.L., Bush, W.S., Engelman, C.D., Lu, Q., Fardo, D.W., Trittschuh, E.H., Mez, J., et al. (2020). Genetic variants and functional pathways associated with resilience to Alzheimer's disease. Brain *143*, 2561–2575. https://doi.org/10.1093/brain/awaa209.
3. Mayeux, R., and Stern, Y. (2012). Epidemiology of Alzheimer disease. Cold Spring Harb. Perspect. Med. *2*, a006239. https://doi.org/10.1101/cshperspect.a006239.
4. Reitz, C., and Mayeux, R. (2009). Use of genetic variation as biomarkers for Alzheimer's disease. Ann. N. Y. Acad. Sci. *1180*, 75–96. https://doi.org/10.1111/j.1749-6632.2009.04945.x.
5. Bellenguez, C., Kucukali, F., Jansen, I.E., Kleineidam, L., Moreno-Grau, S., Amin, N., Naj, A.C., Campos-Martin, R., Grenier-Boley, B., Andrade, V., et al. (2022). New insights into the genetic etiology of Alzheimer's disease and related dementias. Nat. Genet. *54*, 412–436. https://doi.org/10.1038/s41588-022-01024-z.
6. Bhattarai, P., Gunasekaran, T.I., Belloy, M.E., Reyes-Dumeyer, D., Jülich, D., Tayran, H., Yilmaz, E., Flaherty, D., Turgutalp, B., Sukumar, G., et al. (2024). Rare genetic variation in fibronectin 1 (FN1) protects against APOEepsilon4 in Alzheimer's disease. Acta Neuropathol. *147*, 70. https://doi.org/10.1007/s00401-024-02721-1.
7. Murdock, M.H., and Tsai, L.H. (2023). Insights into Alzheimer's disease from single-cell genomic approaches. Nat. Neurosci. *26*, 181–195. https://doi.org/10.1038/s41593-022-01222-2.
8. Bhattarai, P., Turgutalp, B., and Kizil, C. (2022). Zebrafish as an Experimental and Preclinical Model for Alzheimer's Disease. ACS Chem. Neurosci. *13*, 2939–2941. https://doi.org/10.1021/acschemneuro.2c00583.
9. Siddiqui, T., Bhattarai, P., Popova, S., Cosacak, M.I., Sariya, S., Zhang, Y., Mayeux, R., Tosto, G., and Kizil, C. (2021). KYNA/Ahr Signaling Suppresses Neural Stem Cell Plasticity and Neurogenesis in Adult Zebrafish Model of Alzheimer's Disease. Cells *10*, 2748. https://doi.org/10.3390/cells10102748.
10. Bhattarai, P., Cosacak, M.I., Mashkaryan, V., Demir, S., Popova, S.D., Govindarajan, N., Brandt, K., Zhang, Y., Chang, W., Ampatzis, K., and Kizil, C. (2020). Neuron-glia interaction through Serotonin-BDNF-NGFR axis enables regenerative neurogenesis in Alzheimer's model of adult zebrafish brain. PLoS Biol. *18*, e3000585. https://doi.org/10.1371/journal.pbio.3000585.
11. Cosacak, M.I., Bhattarai, P., Reinhardt, S., Petzold, A., Dahl, A., Zhang, Y., and Kizil, C. (2019). Single-Cell Transcriptomics Analyses of Neural Stem Cell Heterogeneity and Contextual Plasticity in a Zebrafish Brain Model of Amyloid Toxicity. Cell Rep. *27*, 1307–1318.e3. https://doi.org/10.1016/j.celrep.2019.03.090.
12. Bhattarai, P., Thomas, A.K., Zhang, Y., and Kizil, C. (2017). The effects of aging on Amyloid-β42-induced neurodegeneration and regeneration in adult zebrafish brain. Neurogenesis *4*, e1322666. https://doi.org/10.1080/23262133.2017.1322666.
13. Cosacak, M.I., Bhattarai, P., Bocova, L., Dzewas, T., Mashkaryan, V., Papadimitriou, C., Brandt, K., Hollak, H., Antos, C.L., and Kizil, C. (2017). Human TAUP301L overexpression results in TAU hyperphosphorylation without neurofibrillary tangles in adult zebrafish. Sci. Rep. *7*, 12959. https://doi.org/10.1038/s41598-017-13311-5.
14. Bhattarai, P., Thomas, A.K., Cosacak, M.I., Papadimitriou, C., Mashkaryan, V., Zhang, Y., and Kizil, C. (2017). Modeling Amyloid-β42 Toxicity and Neurodegeneration in Adult Zebrafish Brain. J. Vis. Exp. *128*, 56014. https://doi.org/10.3791/56014.
15. Bhattarai, P., Thomas, A.K., Cosacak, M.I., Papadimitriou, C., Mashkaryan, V., Froc, C., Reinhardt, S., Kurth, T., Dahl, A., Zhang, Y., and Kizil, C. (2016). IL4/STAT6 signaling activates neural stem cell proliferation and neurogenesis upon Amyloid-β42 aggregation in adult zebrafish brain. Cell Rep. *17*, 941–948. https://doi.org/10.1016/j.celrep.2016.09.075.
16. Kizil, C., Sariya, S., Kim, Y.A., Rajabli, F., Martin, E., Reyes-Dumeyer, D., Vardarajan, B., Maldonado, A., Haines, J.L., Mayeux, R., et al. (2022). Admixture Mapping of Alzheimer's disease in Caribbean Hispanics identifies a new locus on 22q13.1. Mol. Psychiatry *27*, 2813–2820. https://doi.org/10.1038/s41380-022-01526-6.
17. Lee, A.J., Raghavan, N.S., Bhattarai, P., Siddiqui, T., Sariya, S., Reyes-Dumeyer, D., Flowers, X.E., Cardoso, S.A.L., De Jager, P.L., Bennett, D.A., et al. (2022). FMNL2 regulates gliovascular interactions and is associated with vascular risk factors and cerebrovascular pathology in Alzheimer's disease. Acta Neuropathol. *144*, 59–79. https://doi.org/10.1007/s00401-022-02431-6.
18. Ray, N.R., Kunkle, B.W., Hamilton-Nelson, K., Kurup, J.T., Rajabli, F., Qiao, M., Vardarajan, B.N., Cosacak, M.I., Kizil, C., Jean-Francois, M., et al. (2024). Extended genome-wide association study employing the African genome resources panel identifies novel susceptibility loci for Alzheimer's disease in individuals of African ancestry. Alzheimers Dement. https://doi.org/10.1002/alz.13880.
19. Is, O., Wang, X., Reddy, J., Min, Y., Yilmaz, E., Bhattarai, P., Patel, T., Bergman, J., Quicksall, Z., Heckman, M., et al. (2024). Gliovascular transcriptional perturbations in Alzheimer's disease reveal molecular mechanisms of blood brain barrier dysfunction. Nat. Commun. *15*, 4758. https://doi.org/10.1038/s41467-024-48926-6.

20. Turgutalp, B., Bhattarai, P., Ercetin, T., Luise, C., Reis, R., Gurdal, E., Isaak, A., Biriken, D., Dinter, E., Sipahi, H., et al. (2022). Discovery of Potent Cholinesterase Inhibition-Based Multi-Target-Directed Lead Compounds for Synaptoprotection in Alzheimer's Disease. J. Med. Chem. *65*, 12292–12318.

21. Reinhardt, L., Kordes, S., Reinhardt, P., Glatza, M., Baumann, M., Drexler, H.C.A., Menninger, S., Zischinsky, G., Eickhoff, J., Fröb, C., et al. (2019). Dual Inhibition of GSK3beta and CDK5 Protects the Cytoskeleton of Neurons from Neuroinflammatory-Mediated Degeneration In Vitro and In Vivo. Stem Cell Rep. *12*, 502–517. https://doi.org/10.1016/j.stemcr.2019.01.015.

22. Haage, V., Tuddenham, J.F., Comandante-Lou, N., Bautista, A., Monzel, A., Chiu, R., Fujita, M., Garcia, F.G., Bhattarai, P., Patel, R., et al. (2024). A pharmacological toolkit for human microglia identifies Topoisomerase I inhibitors as immunomodulators for Alzheimer's disease. bioRxiv. https://doi.org/10.1101/2024.02.06.579103.

23. Turgutalp, B., and Kizil, C. (2024). Multi-target drugs for Alzheimer's disease. Trends Pharmacol. Sci. *45*, 628–638. https://doi.org/10.1016/j.tips.2024.05.005.

24. Cosacak, M.I., Bhattarai, P., and Kizil, C. (2020). Alzheimer's disease, neural stem cells and neurogenesis: cellular phase at single-cell level. Neural Reg Res *15*, 824–827. https://doi.org/10.4103/1673-5374.268896.

25. Jurisch-Yaksi, N., Yaksi, E., and Kizil, C. (2020). Radial glia in the zebrafish brain: Functional, structural, and physiological comparison with the mammalian glia. Glia *68*, 2451–2470. https://doi.org/10.1002/glia.23849.

26. Kizil, C. (2018). Mechanisms of Pathology-Induced Neural Stem Cell Plasticity and Neural Regeneration in Adult Zebrafish Brain. Curr. Pathobiol. Rep. *6*, 71–77. https://doi.org/10.1007/s40139-018-0158-x.

27. Kizil, C., and Bhattarai, P. (2018). Is Alzheimer's Also a Stem Cell Disease? - The Zebrafish Perspective. Front. Cell Dev. Biol. *6*, 159. https://doi.org/10.3389/fcell.2018.00159.

28. Tincer, G., Mashkaryan, V., Bhattarai, P., and Kizil, C. (2016). Neural stem/progenitor cells in Alzheimer's disease. Yale J. Biol. Med. *89*, 23–35.

29. Siddiqui, T., Celikkaya, H., Atasavum, Z.T., Popova, S., Freudenberg, U., Werner, C., and Kizil, C. (2023). Three-Dimensional Biohybrid StarPEG-Heparin Hydrogel Cultures for Modeling Human Neuronal Development and Alzheimer's Disease Pathology. Methods Mol. Biol. *2561*, 159–170. https://doi.org/10.1007/978-1-0716-2655-9_8.

30. Siddiqui, T., Cosacak, M.I., Popova, S., Bhattarai, P., Yilmaz, E., Lee, A.J., Min, Y., Wang, X., Allen, M., İş, Ö., et al. (2023). Nerve growth factor receptor (Ngfr) induces neurogenic plasticity by suppressing reactive astroglial Lcn2/Slc22a17 signaling in Alzheimer's disease. NPJ Regen. Med. *8*, 33. https://doi.org/10.1038/s41536-023-00311-5.

31. Mashkaryan, V., Siddiqui, T., Popova, S., Cosacak, M.I., Bhattarai, P., Brandt, K., Govindarajan, N., Petzold, A., Reinhardt, S., Dahl, A., et al. (2020). Type 1 Interleukin-4 signaling obliterates mouse astroglia in vivo but not in vitro. Front. Cell Dev. Biol. *8*, 114. https://doi.org/10.3389/fcell.2020.00114.

32. Celikkaya, H., Cosacak, M.I., Papadimitriou, C., Popova, S., Bhattarai, P., Biswas, S.N., Siddiqui, T., Wistorf, S., Nevado-Alcalde, I., Naumann, L., et al. (2019). GATA3 Promotes the Neural Progenitor State but Not Neurogenesis in 3D Traumatic Injury Model of Primary Human Cortical Astrocytes. Front. Cell. Neurosci. *13*, 23. https://doi.org/10.3389/fncel.2019.00023.

33. Papadimitriou, C., Celikkaya, H., Cosacak, M.I., Mashkaryan, V., Bray, L., Bhattarai, P., Brandt, K., Hollak, H., Chen, X., He, S., et al. (2018). 3D Culture Method for Alzheimer's Disease Modeling Reveals Interleukin-4 Rescues Abeta42-Induced Loss of Human Neural Stem Cell Plasticity. Dev. Cell *46*, 85–101.e108. https://doi.org/10.1016/j.devcel.2018.06.005.

34. Zhang, X.Y., Wang, Y.F., Zheng, L.J., Zhang, H., Lin, L., Lu, G.M., and Zhang, L.J. (2020). Impacts of AD-Related ABCA7 and CLU Variants on Default Mode Network Connectivity in Healthy Middle-Age Adults. Front. Mol. Neurosci. *13*, 145. https://doi.org/10.3389/fnmol.2020.00145.

35. De Roeck, A., Van Broeckhoven, C., and Sleegers, K. (2019). The role of ABCA7 in Alzheimer's disease: evidence from genomics, transcriptomics and methylomics. Acta Neuropathol. *138*, 201–220. https://doi.org/10.1007/s00401-019-01994-1.

36. Aikawa, T., Holm, M.L., and Kanekiyo, T. (2018). ABCA7 and Pathogenic Pathways of Alzheimer's Disease. Brain Sci. *8*, 27. https://doi.org/10.3390/brainsci8020027.

37. Allen, M., Lincoln, S.J., Corda, M., Watzlawik, J.O., Carrasquillo, M.M., Reddy, J.S., Burgess, J.D., Nguyen, T., Malphrus, K., Petersen, R.C., et al. (2017). ABCA7 loss-of-function variants, expression, and neurologic disease risk. Neurol. Genet. *3*, e126. https://doi.org/10.1212/NXG.0000000000000126.

38. Hohman, T.J., Cooke-Bailey, J.N., Reitz, C., Jun, G., Naj, A., Beecham, G.W., Liu, Z., Carney, R.M., Vance, J.M., Cuccaro, M.L., et al. (2016). Global and local ancestry in African-Americans: Implications for Alzheimer's disease risk. Alzheimers Dement. *12*, 233–243. https://doi.org/10.1016/j.jalz.2015.02.012.

39. Reitz, C., Jun, G., Naj, A., Rajbhandary, R., Vardarajan, B.N., Wang, L.S., Valladares, O., Lin, C.F., Larson, E.B., Graff-Radford, N.R., et al. (2013). Variants in the ATP-binding cassette transporter (ABCA7), apolipoprotein E ϵ4,and the risk of late-onset Alzheimer disease in African Americans. JAMA *309*, 1483–1492. https://doi.org/10.1001/jama.2013.2973.

40. Campbell, A.S., Ho, C.C.G., Atık, M., Allen, M., Lincoln, S., Malphrus, K., Nguyen, T., Oatman, S.R., Corda, M., Conway, O., et al. (2022). Clinical Deep Phenotyping of ABCA7 Mutation Carriers. Neurol. Genet. *8*, e655. https://doi.org/10.1212/NXG.0000000000000655.

41. N'Songo, A., Carrasquillo, M.M., Wang, X., Burgess, J.D., Nguyen, T., Asmann, Y.W., Serie, D.J., Younkin, S.G., Allen, M., Pedraza, O., et al. (2017). African American exome sequencing identifies potential risk variants at Alzheimer disease loci. Neurol. Genet. *3*, e141. https://doi.org/10.1212/NXG.0000000000000141.

42. Carrasquillo, M.M., Crook, J.E., Pedraza, O., Thomas, C.S., Pankratz, V.S., Allen, M., Nguyen, T., Malphrus, K.G., Ma, L., Bisceglio, G.D., et al. (2015). Late-onset Alzheimer's risk variants in memory decline, incident mild cognitive impairment, and Alzheimer's disease. Neurobiol. Aging *36*, 60–67. https://doi.org/10.1016/j.neurobiolaging.2014.07.042.

43. Carrasquillo, M.M., Khan, Q.u.A., Murray, M.E., Krishnan, S., Aakre, J., Pankratz, V.S., Nguyen, T., Ma, L., Bisceglio, G., Petersen, R.C., et al. (2014). Late-onset Alzheimer disease genetic variants in posterior cortical atrophy and posterior AD. Neurology *82*, 1455–1462. https://doi.org/10.1212/WNL.0000000000000335.

44. Aikawa, T., Ren, Y., Holm, M.L., Asmann, Y.W., Alam, A., Fitzgerald, M.L., Bu, G., and Kanekiyo, T. (2021). ABCA7 Regulates Brain Fatty Acid Metabolism During LPS-Induced Acute Inflammation. Front. Neurosci. *15*, 647974. https://doi.org/10.3389/fnins.2021.647974.

45. Sakae, N., Liu, C.C., Shinohara, M., Frisch-Daiello, J., Ma, L., Yamazaki, Y., Tachibana, M., Younkin, L., Kurti, A., Carrasquillo, M.M., et al. (2016). ABCA7 Deficiency Accelerates Amyloid-beta Generation and Alzheimer's Neuronal Pathology. J. Neurosci. *36*, 3848–3859. https://doi.org/10.1523/JNEUROSCI.3757-15.2016.

46. Lyssenko, N.N., and Praticò, D. (2021). ABCA7 and the altered lipidostasis hypothesis of Alzheimer's disease. Alzheimers Dement. *17*, 164–174. https://doi.org/10.1002/alz.12220.

47. Nowyhed, H.N., Chandra, S., Kiosses, W., Marcovecchio, P., Andary, F., Zhao, M., Fitzgerald, M.L., Kronenberg, M., and Hedrick, C.C. (2017). ATP Binding Cassette Transporter ABCA7 Regulates NKT Cell Development and Function by Controlling CD1d Expression and Lipid Raft Content. Sci. Rep. *7*, 40273. https://doi.org/10.1038/srep40273.

48. Kaminski, W.E., Orsó, E., Diederich, W., Klucken, J., Drobnik, W., and Schmitz, G. (2000). Identification of a novel human sterol-sensitive

ATP-binding cassette transporter (ABCA7). Biochem. Biophys. Res. Commun. *273*, 532–538. https://doi.org/10.1006/bbrc.2000.2954.

49. Kawatani, K., Holm, M.L., Starling, S.C., Martens, Y.A., Zhao, J., Lu, W., Ren, Y., Li, Z., Jiang, P., Jiang, Y., et al. (2024). ABCA7 deficiency causes neuronal dysregulation by altering mitochondrial lipid metabolism. Mol. Psychiatry *29*, 809–819. https://doi.org/10.1038/s41380-023-02372-w.
50. Moulton, M.J., Barish, S., Ralhan, I., Chang, J., Goodman, L.D., Harland, J.G., Marcogliese, P.C., Johansson, J.O., Ioannou, M.S., and Bellen, H.J. (2021). Neuronal ROS-induced glial lipid droplet formation is altered by loss of Alzheimer's disease-associated genes. Proc. Natl. Acad. Sci. USA *118*, e2112095118. https://doi.org/10.1073/pnas.2112095118.
51. Kim, W.S., Li, H., Ruberu, K., Chan, S., Elliott, D.A., Low, J.K., Cheng, D., Karl, T., and Garner, B. (2013). Deletion of Abca7 increases cerebral amyloid-beta accumulation in the J20 mouse model of Alzheimer's disease. J. Neurosci. *33*, 4387–4394. https://doi.org/10.1523/JNEUROSCI.4165-12.2013.
52. Cukier, H.N., Kunkle, B.W., Vardarajan, B.N., Rolati, S., Hamilton-Nelson, K.L., Kohli, M.A., Whitehead, P.L., Dombroski, B.A., Van Booven, D., Lang, R., et al. (2016). ABCA7 frameshift deletion associated with Alzheimer disease in African Americans. Neurol. Genet. *2*, e79. https://doi.org/10.1212/NXG.0000000000000079.
53. Steinberg, S., Stefansson, H., Jonsson, T., Johannsdottir, H., Ingason, A., Helgason, H., Sulem, P., Magnusson, O.T., Gudjonsson, S.A., Unsteinsdottir, U., et al. (2015). Loss-of-function variants in ABCA7 confer risk of Alzheimer's disease. Nat. Genet. *47*, 445–447. https://doi.org/10.1038/ng.3246.
54. Cuyvers, E., De Roeck, A., Van den Bossche, T., Van Cauwenberghe, C., Bettens, K., Vermeulen, S., Mattheijssens, M., Peeters, K., Engelborghs, S., Vandenbulcke, M., et al. (2015). Mutations in ABCA7 in a Belgian cohort of Alzheimer's disease patients: a targeted resequencing study. Lancet Neurol. *14*, 814–822. https://doi.org/10.1016/S1474-4422(15)00133-7.
55. Davis, A., Gao, R., and Navin, N.E. (2019). SCOPIT: sample size calculations for single-cell sequencing experiments. BMC Bioinf. *20*, 566. https://doi.org/10.1186/s12859-019-3167-9.
56. Schmid, K.T., Höllbacher, B., Cruceanu, C., Böttcher, A., Lickert, H., Binder, E.B., Theis, F.J., and Heinig, M. (2021). scPower accelerates and optimizes the design of multi-sample single cell transcriptomic studies. Nat. Commun. *12*, 6625. https://doi.org/10.1038/s41467-021-26779-7.
57. Kielar, D., Kaminski, W.E., Liebisch, G., Piehler, A., Wenzel, J.J., Möhle, C., Heimerl, S., Langmann, T., Friedrich, S.O., Böttcher, A., et al. (2003). Adenosine triphosphate binding cassette (ABC) transporters are expressed and regulated during terminal keratinocyte differentiation: a potential role for ABCA7 in epidermal lipid reorganization. J. Invest. Dermatol. *121*, 465–474. https://doi.org/10.1046/j.1523-1747.2003.12404.x.
58. Cosacak, M.I., Bhattarai, P., De Jager, P.L., Menon, V., Tosto, G., and Kizil, C. (2022). Single Cell/Nucleus Transcriptomics Comparison in Zebrafish and Humans Reveals Common and Distinct Molecular Responses to Alzheimer's Disease. Cells *11*, 1807. https://doi.org/10.3390/cells11111807.
59. Rodriguez, J.J., and Verkhratsky, A. (2011). Neurogenesis in Alzheimer's disease. J. Anat. *219*, 78–89. https://doi.org/10.1111/j.1469-7580.2011.01343.x.
60. Lau, S.F., Cao, H., Fu, A.K.Y., and Ip, N.Y. (2020). Single-nucleus transcriptome analysis reveals dysregulation of angiogenic endothelial cells and neuroprotective glia in Alzheimer's disease. Proc. Natl. Acad. Sci. USA *117*, 25800–25809. https://doi.org/10.1073/pnas.2008762117.
61. Kim, Y.A., Mellen, M., Kizil, C., and Santa-Maria, I. (2024). Mechanisms linking cerebrovascular dysfunction and tauopathy: Adding a layer of epiregulatory complexity. Br. J. Pharmacol. *181*, 879–895. https://doi.org/10.1111/bph.16280.
62. Felsky, D., Santa-Maria, I., Cosacak, M.I., French, L., Schneider, J.A., Bennett, D.A., De Jager, P.L., Kizil, C., and Tosto, G. (2023). The Caribbean-Hispanic Alzheimer's disease brain transcriptome reveals ancestry-specific disease mechanisms. Neurobiol. Dis. *176*, 105938. https://doi.org/10.1016/j.nbd.2022.105938.
63. Leng, K., Li, E., Eser, R., Piergies, A., Sit, R., Tan, M., Neff, N., Li, S.H., Rodriguez, R.D., Suemoto, C.K., et al. (2021). Molecular characterization of selectively vulnerable neurons in Alzheimer's disease. Nat. Neurosci. *24*, 276–287. https://doi.org/10.1038/s41593-020-00764-7.
64. Allen, M., Wang, X., Burgess, J.D., Watzlawik, J., Serie, D.J., Younkin, C.S., Nguyen, T., Malphrus, K.G., Lincoln, S., Carrasquillo, M.M., et al. (2018). Conserved brain myelination networks are altered in Alzheimer's and other neurodegenerative diseases. Alzheimers Dement. *14*, 352–366. https://doi.org/10.1016/j.jalz.2017.09.012.
65. Allen, M., Carrasquillo, M.M., Funk, C., Heavner, B.D., Zou, F., Younkin, C.S., Burgess, J.D., Chai, H.S., Crook, J., Eddy, J.A., et al. (2016). Human whole genome genotype and transcriptome data for Alzheimer's and other neurodegenerative diseases. Sci. Data *3*, 160089. https://doi.org/10.1038/sdata.2016.89.
66. Wang, M., Beckmann, N.D., Roussos, P., Wang, E., Zhou, X., Wang, Q., Ming, C., Neff, R., Ma, W., Fullard, J.F., et al. (2018). The Mount Sinai cohort of large-scale genomic, transcriptomic and proteomic data in Alzheimer's disease. Sci. Data *5*, 180185. https://doi.org/10.1038/sdata.2018.185.
67. De Jager, P.L., Ma, Y., McCabe, C., Xu, J., Vardarajan, B.N., Felsky, D., Klein, H.U., White, C.C., Peters, M.A., Lodgson, B., et al. (2018). A multi-omic atlas of the human frontal cortex for aging and Alzheimer's disease research. Sci. Data *5*, 180142. https://doi.org/10.1038/sdata.2018.142.
68. Mathys, H., Peng, Z., Boix, C.A., Victor, M.B., Leary, N., Babu, S., Abdelhady, G., Jiang, X., Ng, A.P., Ghafari, K., et al. (2023). Single-cell atlas reveals correlates of high cognitive function, dementia, and resilience to Alzheimer's disease pathology. Cell *186*, 4365–4385.e27. https://doi.org/10.1016/j.cell.2023.08.039.
69. Browaeys, R., Saelens, W., and Saeys, Y. (2020). NicheNet: modeling intercellular communication by linking ligands to target genes. Nat. Methods *17*, 159–162. https://doi.org/10.1038/s41592-019-0667-5.
70. Reyes-Dumeyer, D., Faber, K., Vardarajan, B., Goate, A., Renton, A., Chao, M., Boeve, B., Cruchaga, C., Pericak-Vance, M., Haines, J.L., et al. (2022). The National Institute on Aging Late-Onset Alzheimer's Disease Family Based Study: A resource for genetic discovery. Alzheimers Dement. *18*, 1889–1897. https://doi.org/10.1002/alz.12514.
71. Vardarajan, B.N., Faber, K.M., Bird, T.D., Bennett, D.A., Rosenberg, R., Boeve, B.F., Graff-Radford, N.R., Goate, A.M., Farlow, M., Sweet, R.A., et al. (2014). Age-specific incidence rates for dementia and Alzheimer disease in NIA-LOAD/NCRAD and EFIGA families: National Institute on Aging Genetics Initiative for Late-Onset Alzheimer Disease/National Cell Repository for Alzheimer Disease (NIA-LOAD/NCRAD) and Estudio Familiar de Influencia Genetica en Alzheimer (EFIGA). JAMA Neurol. *71*, 315–323. https://doi.org/10.1001/jamaneurol.2013.5570.
72. Duron, E., Vidal, J.S., Grousselle, D., Gabelle, A., Lehmann, S., Pasquier, F., Bombois, S., Buée, L., Allinquant, B., Schraen-Maschke, S., et al. (2018). Somatostatin and Neuropeptide Y in Cerebrospinal Fluid: Correlations With Amyloid Peptides Abeta(1-42) and Tau Proteins in Elderly Patients With Mild Cognitive Impairment. Front. Aging Neurosci. *10*, 297. https://doi.org/10.3389/fnagi.2018.00297.
73. Unger, M.S., Marschallinger, J., Kaindl, J., Höfling, C., Rossner, S., Heneka, M.T., Van der Linden, A., and Aigner, L. (2016). Early Changes in Hippocampal Neurogenesis in Transgenic Mouse Models for Alzheimer's Disease. Mol. Neurobiol. *53*, 5796–5806. https://doi.org/10.1007/s12035-016-0018-9.
74. Spencer, B., Potkar, R., Metcalf, J., Thrin, I., Adame, A., Rockenstein, E., and Masliah, E. (2016). Systemic Central Nervous System (CNS)-targeted Delivery of Neuropeptide Y (NPY) Reduces Neurodegeneration and Increases Neural Precursor Cell Proliferation in a Mouse Model of Alzheimer Disease. J. Biol. Chem. *291*, 1905–1920. https://doi.org/10.1074/jbc.M115.678185.

75. Juhasz, G., Hullam, G., Eszlari, N., Gonda, X., Antal, P., Anderson, I.M., Hökfelt, T.G.M., Deakin, J.F.W., and Bagdy, G. (2014). Brain galanin system genes interact with life stresses in depression-related phenotypes. Proc. Natl. Acad. Sci. USA *111*, E1666–E1673. https://doi.org/10.1073/pnas.1403649111.

76. Croce, N., Gelfo, F., Ciotti, M.T., Federici, G., Caltagirone, C., Bernardini, S., and Angelucci, F. (2013). NPY modulates miR-30a-5p and BDNF in opposite direction in an in vitro model of Alzheimer disease: a possible role in neuroprotection? Mol. Cell. Biochem. *376*, 189–195. https://doi.org/10.1007/s11010-013-1567-0.

77. Rose, J.B., Crews, L., Rockenstein, E., Adame, A., Mante, M., Hersh, L.B., Gage, F.H., Spencer, B., Potkar, R., Marr, R.A., and Masliah, E. (2009). Neuropeptide Y fragments derived from neprilysin processing are neuroprotective in a transgenic model of Alzheimer's disease. J. Neurosci. *29*, 1115–1125. https://doi.org/10.1523/JNEUROSCI.4220-08.2009.

78. Xapelli, S., Bernardino, L., Ferreira, R., Grade, S., Silva, A.P., Salgado, J.R., Cavadas, C., Grouzmann, E., Poulsen, F.R., Jakobsen, B., et al. (2008). Interaction between neuropeptide Y (NPY) and brain-derived neurotrophic factor in NPY-mediated neuroprotection against excitotoxicity: a role for microglia. Eur. J. Neurosci. *27*, 2089–2102. https://doi.org/10.1111/j.1460-9568.2008.06172.x.

79. Wirth, M.J., Patz, S., and Wahle, P. (2005). Transcellular induction of neuropeptide Y expression by NT4 and BDNF. Proc. Natl. Acad. Sci. USA *102*, 3064–3069. https://doi.org/10.1073/pnas.0404712102.

80. Reaux, A., De Mota, N., Skultetyova, I., Lenkei, Z., El Messari, S., Gallatz, K., Corvol, P., Palkovits, M., and Llorens-Cortès, C. (2001). Physiological role of a novel neuropeptide, apelin, and its receptor in the rat brain. J. Neurochem. *77*, 1085–1096.

81. Adrian, T.E., Allen, J.M., Bloom, S.R., Ghatei, M.A., Rossor, M.N., Roberts, G.W., Crow, T.J., Tatemoto, K., and Polak, J.M. (1983). Neuropeptide Y distribution in human brain. Nature *306*, 584–586. https://doi.org/10.1038/306584a0.

82. Chan-Palay, V., Lang, W., Haesler, U., Köhler, C., and Yasargil, G. (1986). Distribution of altered hippocampal neurons and axons immunoreactive with antisera against neuropeptide Y in Alzheimer's-type dementia. J. Comp. Neurol. *248*, 376–394. https://doi.org/10.1002/cne.902480307.

83. Chan-Palay, V., and Yasargil, G. (1986). Immunocytochemistry of human brain tissue with a polyclonal antiserum against neuropeptide Y. Anat. Embryol. *174*, 27–33. https://doi.org/10.1007/BF00318333.

84. Chan-Palay, V., Lang, W., Allen, Y.S., Haesler, U., and Polak, J.M. (1985). Cortical neurons immunoreactive with antisera against neuropeptide Y are altered in Alzheimer's-type dementia. J. Comp. Neurol. *238*, 390–400. https://doi.org/10.1002/cne.902380404.

85. Nilsson, C.L., Brinkmalm, A., Minthon, L., Blennow, K., and Ekman, R. (2001). Processing of neuropeptide Y, galanin, and somatostatin in the cerebrospinal fluid of patients with Alzheimer's disease and frontotemporal dementia. Peptides *22*, 2105–2112. https://doi.org/10.1016/s0196-9781(01)00571-x.

86. Lilja, A.M., Malmsten, L., Röjdner, J., Voytenko, L., Verkhratsky, A., Ögren, S.O., Nordberg, A., and Marutle, A. (2015). Neural Stem Cell Transplant-Induced Effect on Neurogenesis and Cognition in Alzheimer Tg2576 Mice Is Inhibited by Concomitant Treatment with Amyloid-Lowering or Cholinergic $\alpha 7$ Nicotinic Receptor Drugs. Neural Plast. *2015*, 370432. https://doi.org/10.1155/2015/370432.

87. Hong, J.Y., Lee, S.H., Lee, S.C., Kim, J.W., Kim, K.P., Kim, S.M., Tapia, N., Lim, K.T., Kim, J., Ahn, H.S., et al. (2014). Therapeutic potential of induced neural stem cells for spinal cord injury. J. Biol. Chem. *289*, 32512–32525. https://doi.org/10.1074/jbc.M114.588871.

88. Gage, F.H., and Temple, S. (2013). Neural stem cells: generating and regenerating the brain. Neuron *80*, 588–601. https://doi.org/10.1016/j.neuron.2013.10.037.

89. Kizil, C., Kaslin, J., Kroehne, V., and Brand, M. (2012). Adult neurogenesis and brain regeneration in zebrafish. Dev. Neurobiol. *72*, 429–461. https://doi.org/10.1002/dneu.20918.

90. Lopez-Toledano, M.A., and Shelanski, M.L. (2004). Neurogenic effect of beta-amyloid peptide in the development of neural stem cells. J. Neurosci. *24*, 5439–5444. https://doi.org/10.1523/JNEUROSCI.0974-04.2004.

91. Doetsch, F., and Scharff, C. (2001). Challenges for brain repair: insights from adult neurogenesis in birds and mammals. Brain Behav. Evol. *58*, 306–322. 57572 [pii].

92. Wyss-Coray, T. (2016). Ageing, neurodegeneration and brain rejuvenation. Nature *539*, 180–186. https://doi.org/10.1038/nature20411.

93. Choi, S.H., and Tanzi, R.E. (2019). Is Alzheimer's Disease a Neurogenesis Disorder? Cell Stem Cell *25*, 7–8. https://doi.org/10.1016/j.stem.2019.06.001.

94. Tobin, M.K., Musaraca, K., Disouky, A., Shetti, A., Bheri, A., Honer, W.G., Kim, N., Dawe, R.J., Bennett, D.A., Arfanakis, K., and Lazarov, O. (2019). Human Hippocampal Neurogenesis Persists in Aged Adults and Alzheimer's Disease Patients. Cell Stem Cell *24*, 974–982.e3. https://doi.org/10.1016/j.stem.2019.05.003.

95. Moreno-Jimenez, E.P., Flor-Garcia, M., Terreros-Roncal, J., Rabano, A., Cafini, F., Pallas-Bazarra, N., Avila, J., and Llorens-Martin, M. (2019). Adult hippocampal neurogenesis is abundant in neurologically healthy subjects and drops sharply in patients with Alzheimer's disease. Nat Med *25*, 554–560. https://doi.org/10.1038/s41591-019-0375-9.

96. Choi, S.H., Bylykbashi, E., Chatila, Z.K., Lee, S.W., Pulli, B., Clemenson, G.D., Kim, E., Rompala, A., Oram, M.K., Asselin, C., et al. (2018). Combined adult neurogenesis and BDNF mimic exercise effects on cognition in an Alzheimer's mouse model. Science *361*, eaan8821. https://doi.org/10.1126/science.aan8821.

97. Wu, A., Wojtowicz, K., Savary, S., Hamon, Y., and Trombik, T. (2020). Do ABC transporters regulate plasma membrane organization? Cell. Mol. Biol. Lett. *25*, 37. https://doi.org/10.1186/s11658-020-00224-x.

98. Dyck, M., Kerth, A., Blume, A., and Lösche, M. (2006). Interaction of the neurotransmitter, neuropeptide Y, with phospholipid membranes: infrared spectroscopic characterization at the air/water interface. J. Phys. Chem. B *110*, 22152–22159. https://doi.org/10.1021/jp062537q.

99. Redd, M.J., Kelly, G., Dunn, G., Way, M., and Martin, P. (2006). Imaging macrophage chemotaxis in vivo: studies of microtubule function in zebrafish wound inflammation. Cell Motil Cytoskeleton *63*, 415–422. https://doi.org/10.1002/cm.20133.

100. Kanther, M., Sun, X., Muhlbauer, M., Mackey, L.C., Flynn, E.J., Bagnat, M., Jobin, C., and Rawls, J.F. (2011). Microbial colonization induces dynamic temporal and spatial patterns of NF-kappaB activation in the zebrafish digestive tract. Gastroenterology *141*, 197–207. https://doi.org/10.1053/j.gastro.2011.03.042.

101. Butler, A., Hoffman, P., Smibert, P., Papalexi, E., and Satija, R. (2018). Integrating single-cell transcriptomic data across different conditions, technologies, and species. Nat. Biotechnol. *36*, 411–420. https://doi.org/10.1038/nbt.4096.

102. Faul, F., Erdfelder, E., Buchner, A., and Lang, A.G. (2009). Statistical power analyses using G*Power 3.1: tests for correlation and regression analyses. Behav. Res. Methods *41*, 1149–1160. https://doi.org/10.3758/BRM.41.4.1149.

103. Meeker, N.D., Hutchinson, S.A., Ho, L., and Trede, N.S. (2007). Method for isolation of PCR-ready genomic DNA from zebrafish tissues. Biotechniques *43*, 610–614. https://doi.org/10.2144/000112619.

104. Lister, J.A., Robertson, C.P., Lepage, T., Johnson, S.L., and Raible, D.W. (1999). nacre encodes a zebrafish microphthalmia-related protein that regulates neural-crest-derived pigment cell fate. Development *126*, 3757–3767. https://doi.org/10.1242/dev.126.17.3757.

105. Cosacak, M.I., Bhattarai, P., and Kizil, C. (2020). Protocol for Dissection and Dissociation of Zebrafish Telencephalon for Single-Cell Sequencing. STAR Protoc. *1*, 100042. https://doi.org/10.1016/j.xpro.2020.100042.

106. Zheng, G.X.Y., Lau, B.T., Schnall-Levin, M., Jarosz, M., Bell, J.M., Hindson, C.M., Kyriazopoulou-Panagiotopoulou, S., Masquelier, D.A., Merrill, L., Terry, J.M., et al. (2016). Haplotyping germline and cancer genomes with high-throughput linked-read sequencing. Nat. Biotechnol. *34*, 303–311. https://doi.org/10.1038/nbt.3432.

107. Zheng, G.X.Y., Terry, J.M., Belgrader, P., Ryvkin, P., Bent, Z.W., Wilson, R., Ziraldo, S.B., Wheeler, T.D., McDermott, G.P., Zhu, J., et al. (2017). Massively parallel digital transcriptional profiling of single cells. Nat. Commun. *8*, 14049. https://doi.org/10.1038/ncomms14049.

108. Raj, B., Wagner, D.E., McKenna, A., Pandey, S., Klein, A.M., Shendure, J., Gagnon, J.A., and Schier, A.F. (2018). Simultaneous single-cell profiling of lineages and cell types in the vertebrate brain. Nat. Biotechnol. *36*, 442–450. https://doi.org/10.1038/nbt.4103.

109. Stuart, T., Butler, A., Hoffman, P., Hafemeister, C., Papalexi, E., Mauck, W.M., Hao, Y., Stoeckius, M., Smibert, P., and Satija, R. (2019). Comprehensive Integration of Single-Cell Data. Cell *177*, 1888–1902.e21. https://doi.org/10.1016/j.cell.2019.05.031.

110. McGinnis, C.S., Murrow, L.M., and Gartner, Z.J. (2019). DoubletFinder: Doublet Detection in Single-Cell RNA Sequencing Data Using Artificial Nearest Neighbors. Cell Syst. *8*, 329–337.e4. https://doi.org/10.1016/j.cels.2019.03.003.

111. Satija, R., Farrell, J.A., Gennert, D., Schier, A.F., and Regev, A. (2015). Spatial reconstruction of single-cell gene expression data. Nat. Biotechnol. *33*, 495–502. https://doi.org/10.1038/nbt.3192.

112. Wan, Y.W., Al-Ouran, R., Mangleburg, C.G., Perumal, T.M., Lee, T.V., Allison, K., Swarup, V., Funk, C.C., Gaiteri, C., Allen, M., et al. (2020). Meta-Analysis of the Alzheimer's Disease Human Brain Transcriptome and Functional Dissection in Mouse Models. Cell Rep. *32*, 107908. https://doi.org/10.1016/j.celrep.2020.107908.

113. Wang, X., Allen, M., Li, S., Quicksall, Z.S., Patel, T.A., Carnwath, T.P., Reddy, J.S., Carrasquillo, M.M., Lincoln, S.J., Nguyen, T.T., et al. (2020). Deciphering cellular transcriptional alterations in Alzheimer's disease brains. Mol. Neurodegener. *15*, 38. https://doi.org/10.1186/s13024-020-00392-6.

114. Langfelder, P., and Horvath, S. (2008). WGCNA: an R package for weighted correlation network analysis. BMC Bioinf. *9*, 559. https://doi.org/10.1186/1471-2105-9-559.

115. Conway, O.J., Carrasquillo, M.M., Wang, X., Bredenberg, J.M., Reddy, J.S., Strickland, S.L., Younkin, C.S., Burgess, J.D., Allen, M., Lincoln, S.J., et al. (2018). ABI3 and PLCG2 missense variants as risk factors for neurodegenerative diseases in Caucasians and African Americans. Mol. Neurodegener. *13*, 53. https://doi.org/10.1186/s13024-018-0289-x.

116. Montine, T.J., Phelps, C.H., Beach, T.G., Bigio, E.H., Cairns, N.J., Dickson, D.W., Duyckaerts, C., Frosch, M.P., Masliah, E., Mirra, S.S., et al. (2012). National Institute on Aging-Alzheimer's Association guidelines for the neuropathologic assessment of Alzheimer's disease: a practical approach. Acta Neuropathol. *123*, 1–11. https://doi.org/10.1007/s00401-011-0910-3.

117. Renthal, W., Boxer, L.D., Hrvatin, S., Li, E., Silberfeld, A., Nagy, M.A., Griffith, E.C., Vierbuchen, T., and Greenberg, M.E. (2018). Characterization of human mosaic Rett syndrome brain tissue by single-nucleus RNA sequencing. Nat. Neurosci. *21*, 1670–1679. https://doi.org/10.1038/s41593-018-0270-6.

118. McKenzie, A.T., Wang, M., Hauberg, M.E., Fullard, J.F., Kozlenkov, A., Keenan, A., Hurd, Y.L., Dracheva, S., Casaccia, P., Roussos, P., and Zhang, B. (2018). Brain Cell Type Specific Gene Expression and Co-expression Network Architectures. Sci. Rep. *8*, 8868, ARTN 8868. https://doi.org/10.1038/s41598-018-27293-5.

119. Ianevski, A., Giri, A.K., and Aittokallio, T. (2022). Fully-automated and ultra-fast cell-type identification using specific marker combinations from single-cell transcriptomic data. Nat. Commun. *13*, 1246. https://doi.org/10.1038/s41467-022-28803-w.

120. Browaeys, R., Saelens, W., and Saeys, Y. (2020). NicheNet: modeling intercellular communication by linking ligands to target genes. Nat. Methods *17*, 159–162. https://doi.org/10.1038/s41592-019-0667-5.

121. Masson, J., Sagné, C., Hamon, M., and El Mestikawy, S. (1999). Neurotransmitter transporters in the central nervous system. Pharmacol. Rev. *51*, 439–464.

122. Pedragosa-Badia, X., Stichel, J., and Beck-Sickinger, A.G. (2013). Neuropeptide Y receptors: how to get subtype selectivity. Front. Endocrinol. *4*, 5. https://doi.org/10.3389/fendo.2013.00005.

123. Vardarajan, B.N., Reyes-Dumeyer, D., Piriz, A.L., Lantigua, R.A., Medrano, M., Rivera, D., Jiménez-Velázquez, I.Z., Martin, E., Pericak-Vance, M.A., Bush, W., et al. (2022). Progranulin mutations in clinical and neuropathological Alzheimer's disease. Alzheimers Dement. *18*, 2458–2467. https://doi.org/10.1002/alz.12567.

124. Taliun, D., Harris, D.N., Kessler, M.D., Carlson, J., Szpiech, Z.A., Torres, R., Taliun, S.A.G., Corvelo, A., Gogarten, S.M., Kang, H.M., et al. (2021). Sequencing of 53,831 diverse genomes from the NHLBI TOPMed Program. Nature *590*, 290–299. https://doi.org/10.1038/s41586-021-03205-y.

125. Gunasekaran, T.I., Reyes-Dumeyer, D., Faber, K.M., Goate, A., Boeve, B., Cruchaga, C., Pericak-Vance, M., Haines, J.L., Rosenberg, R., Tsuang, D., et al. (2024). Identification of Rare Damaging Missense and Loss of Function Variants in GWAS Loci Using Genome Sequencing Data from Two Cohorts of Familial Late-Onset Alzheimer's Disease. medRxiv. https://doi.org/10.1101/2023.12.18.23300145.

126. Heiss, J.A., and Just, A.C. (2019). Improved filtering of DNA methylation microarray data by detection p values and its impact on downstream analyses. Clin. Epigenetics *11*, 15. https://doi.org/10.1186/s13148-019-0615-3.

127. Chen, Y.A., Lemire, M., Choufani, S., Butcher, D.T., Grafodatskaya, D., Zanke, B.W., Gallinger, S., Hudson, T.J., and Weksberg, R. (2013). Discovery of cross-reactive probes and polymorphic CpGs in the Illumina Infinium HumanMethylation450 microarray. Epigenetics *8*, 203–209. https://doi.org/10.4161/epi.23470.

128. McCartney, D.L., Walker, R.M., Morris, S.W., McIntosh, A.M., Porteous, D.J., and Evans, K.L. (2016). Identification of polymorphic and off-target probe binding sites on the Illumina Infinium MethylationEPIC BeadChip. Genom. Data *9*, 22–24. https://doi.org/10.1016/j.gdata.2016.05.012.

129. Zhou, W., Laird, P.W., and Shen, H. (2017). Comprehensive characterization, annotation and innovative use of Infinium DNA methylation BeadChip probes. Nucleic Acids Res. *45*, e22. https://doi.org/10.1093/nar/gkw967.

130. Waldvogel, H.J., Curtis, M.A., Baer, K., Rees, M.I., and Faull, R.L.M. (2006). Immunohistochemical staining of post-mortem adult human brain sections. Nat. Protoc. *1*, 2719–2732. https://doi.org/10.1038/nprot.2006.354.

STAR★METHODS

KEY RESOURCES TABLE

REAGENT or RESOURCE	SOURCE	IDENTIFIER
Antibodies		
Recombinant Anti-Glutamine Synthetase (GS) [EPR13022(B)]	Abcam	Cat# ab176562; RRID:AB_2868472
Anti-PCNA [PC10]	Abcam	Cat# ab29; RRID:AB_303394
SV2	Developmental Studies Hybridoma Bank - DSHB	Cat# SV2; RRID:AB_2315387
L-plastin (Gift by Michael Redd)	Redd et al.[99]	
BDNF (for zebrafish tissue)	Sigma-Aldrich/Chemicon	Cat# AB1534sp
BDNF (for human tissue)	Developmental Studies Hybridoma Bank - DSHB	Cat# BDNF-#9; RRID:AB_2617199
NPY	Sigma-Aldrich	Cat# HPA044572
MAP2 [clone AP20]	Millipore Sigma/Chemicon	Cat# MAB3418X; RRID:AB_571048
Goat anti-Mouse IgG2a Cross-Adsorbed Secondary, Alexa Fluor™ 488	Thermofisher	Cat# A-21131; RRID:AB_2535771
Goat anti-Mouse IgG1 Cross-Adsorbed Secondary, Alexa Fluor™ 488	Thermofisher	Cat# A-21121; RRID:AB_2535764
Goat anti-Mouse IgG (H + L) Cross-Adsorbed Secondary, Alexa Fluor™ 488	Thermofisher	Cat# A-11001; RRID:AB_2534069
Goat anti-Rabbit IgG (H + L) Highly Cross-Adsorbed Secondary, Alexa Fluor™ Plus 555	Thermofisher	Cat# A-32732; RRID:AB_2633281
Biological samples		
Postmortem human brain tissue	New York Bran Bank, this paper	
Chemicals, peptides, and recombinant proteins		
TR-Aβ42	Bhattarai et al.[15]	
β-amyloid 1–42 peptide	Abcam	Cat# ab120301
Recombinant human Neuropeptide-Y	Sigma-Aldrich	Cat# 5017
Recombinant human BDNF protein	R&D Systems	Cat#11166-BD
LM11A-31 dihydrochloride (CAS: 1243259-19-9)	MedChemExpress	Cat# HY-11015
MESAB/Tricaine	Sigma-Aldrich	Cat# A5040
Critical commercial assays		
Neural Tissue Dissociation Kit (P)	Miltenyi Biotec	Cat# 130-092-628
mMESSAGE mMACHINE SP6 kit	Invitrogen	Cat# AM1340
MEGAshortscript T7 kit	Invitrogen	Cat# AM1354
mMESSAGE mMACHINE T3 transcription kit	Invitrogen	Cat# AM1348
10X Chromium system	10X Genomics	Cat# 120237
Chromium i7 multiplex kit	10X Genomics	Cat# 120262
Infinium MethylationEPIC kit	Ilumina	Cat# 20087709
Infinium Global Screening Array-24 v3.0 kit	Ilumina	Cat# 20030772
STEMdiff forebrain neuron differentiation kit	Stemcell Technologies	Cat# 08600
STEMdiff forebrain neuron maturation kit	Stemcell Technologies	Cat# 08605
Human Neuropeptide Y (NPY) ELISA kit	Millipore	Cat# EZHNPY-25K
RNA Pico Chip Assay	Agilent Biotechnologies	Cat# 5067-1513
BCA Assay kit	Pierce	Cat# 23225
Deposited data		
Zebrafish abca7 single cell sequencing raw data	This paper	GEO: GSE244550
Human bulk and single-nucleus RNA-seq data	Is et al.[19]	

(*Continued on next page*)

Continued

REAGENT or RESOURCE	SOURCE	IDENTIFIER
Experimental models: cell lines		
Abca7 knockout patient iPSC-derived neurons (MC0192)	Kawatani et al.[49]	
Experimental models: Organisms/strains		
abca7 knockout zebrafish	This paper	
npy mutant zebrafish	This paper	
Tg(NF-κB:GFP) reporter zebrafish	Kanther et al.[100]	
Oligonucleotides		
abca7_sgRNA56 F: 5′-taatacgactcactataGGG CAAATCAAAAAGTCCATgttttagagctagaa -3′	This paper	
abca7_sgRNA58 F: 5′-taatacgactcactataGGA TCATGGGTCTGGGCTCAgttttagagctagaa -3′	This paper	
Genotyping Rev, universal tail: 5′- AAAAGCACCGACTCGGTGCCAC TTTTT CAAGTTGATAACGGACTA -3′	This paper	
Screening for abca7 deletion Forward: 5′- GAGGCCAAAACGGGAATATATGTG-3	This paper	
Screening for abca7 deletion Reverse: 5′- GTGACCCACATTACCACTGTTTG-3	This paper	
Screening for *npy* deletion Forward: 5′- GAAGATGTGGATGAGCTGGGCA -3′	This paper	
Screening for *npy* deletion Reverse: 5′- GCTCACCTCTGCCTTGTTATGAGG -3′	This paper	
qRT-PCR for iPSCs: *GAPDH*: forward: 5′- GTCTCCTCTGACTTCAACAGCG -3′	This paper	
qRT-PCR for iPSCs: *GAPDH* reverse: 5′- ACCACCCTGTTGCTGTAGCCAA -3′	This paper	
qRT-PCR for iPSCs: *ABCA7*: forward: 5′-CCTTGCACAGCTTGTTGGAG -3′	This paper	
qRT-PCR for iPSCs: *ABCA7* reverse: 5′- CTGCTAGGTCCCCTGACACT -3′	This paper	
qRT-PCR for iPSCs: *NPY*: forward: 5′-CGCTGCGACACTACATCAAC -3′	This paper	
qRT-PCR for iPSCs: *NPY* reverse: 5′-CTCTGGGCTGGATCGTTTTCC -3′	This paper	
qRT-PCR for iPSCs: *SLC17A7*: forward: 5′-CTGGGGCTACATTGTCACTCA -3′	This paper	
qRT-PCR for iPSCs: *SLC17A7* reverse: 5′-GCAAAGCCGAAAACTCTGTTG -3′	This paper	
qRT-PCR for iPSCs: *GAD1*: forward: 5′-GCGGACCCCAATACCACTAAC -3′	This paper	
qRT-PCR for iPSCs: *GAD1* reverse: 5′-CACAAGGCGACTCTTCTCTTC -3′	This paper	
Software and algorithms		
Cell Ranger Single Cell Software Suite	10X Genomics	Version 6.1.2; RRID:SCR_017344
Seurat_4.1.3	Buther et al.[101]	Version 4.1.3; RRID:SCR_007322
R package v4.2.2.1		Version 4.2.2.1
GraphPad Prism		Version 9.5.1; RRID:SCR_002798
Zen software (blue edition v3.2) for Zeiss LSM800	Carl Zeiss	Version 3.2; RRID:SCR_013672
ROSMAP_snRNAseq_PFC code	Mathys et al.[68]	https://github.com/mathyslab7/ROSMAP_snRNAseq_PFC

(*Continued on next page*)

Continued

REAGENT or RESOURCE	SOURCE	IDENTIFIER
G*Power, Release 3.1.9.3.	Faul et al.,[102] https://www.psychologie.hhu.de/arbeitsgruppen/allgemeine-psychologie-und-arbeitspsychologie/gpower	RRID:SCR_013726
Other		
cell strainer 40 μm	Falcon	Cat# 352340
Sytox Blue	Invitrogen	Cat# S34857
Dycle Ruby	Invitrogen	Cat# V10309

EXPERIMENTAL MODEL AND STUDY PARTICIPANT DETAILS

Housing and maintenance of animals

All animal experiments were performed in accordance with the applicable regulations and approved by the Institutional Animal Care and Use Committee (IACUC) at Columbia University and or Norwegian Food Safety Authority. Columbia University has the following accreditations: Columbia University Assurance - #D16-00003 (A3007-01), Columbia University USDA Registration - #21-R-0082, Columbia University AAALAC Accreditation - #000687, Columbia University NYDOH - #A141. The animal care and use program at Columbia University is accredited by the AAALAC International and maintains an Animal Welfare Assurance with the Public Health Service (PHS), Assurance number D16-00003 (A3007-01). Animals were handled with caution to reduce suffering and overall animal numbers.

Randomization

To minimize selection bias, zebrafish were randomly assigned to experimental and control groups, ensuring each fish had an equal chance of placement in any group, thus making the groups comparable at the experiment's start. In experiments with known or potential confounding variables (e.g., age, sex, or batch effects in transgenic lines), a randomized block design was utilized. Zebrafish were grouped into blocks based on known variables, and individuals within each block were then randomly assigned to experimental groups.

Effect sizes

Animal experiment sample sizes were determined with G*Power (https://www.psychologie.hhu.de/arbeitsgruppen/allgemeine-psychologie-und-arbeitspsychologie/gpower). Single cell sequencing sample size was calculated with SCOPIT[55] and detection power for differential expression was analyzed with scPower.[56] Animals from both sexes were used.

Blinding

Samples were blinded to group assignments during outcome evaluations. The person analyzing the results was different from the person conducting the experiments.

Health status

The full-time dedicated veterinary staff has training and experience with the species used in the University research programs and is available 24 h a day, 7 days a week. Animals are checked daily at a minimum, but more frequently as needed. An intensive care unit is available, which provides continuous monitoring and medical care, if needed. Within the University program, the Attending Veterinarian or his delegates are authorized, by the Institutional Official, to intervene to alleviate pain or distress as deemed appropriate. Health status of animals was regularly checked observationally, pathologically, and molecularly. No health issues were detected for the animals used for this study.

Human brain samples

Human brain samples were obtained from New York Brain Bank within institutional regulations of Columbia University. The clinical data analyses conducted at Columbia University and Mayo Clinic were approved by the respective Institutional Review Boards.

Authentication of cell lines

The iPSCs used were previously characterized for pluripotency, differentiation potential, and genetic stability.[49]

METHOD DETAILS

Gene editing and generation of *abca7* knockout zebrafish line

Cas9 mRNA synthesis: The template DNA containing the capped Cas9-mRNA, (pCS2-Cas9) was linearized by *NotI* digestion and then purified by reaction purification kit (Invitrogen). Using mMESSAGE mMACHINE SP6 kit (Invitrogen), capped Cas9-mRNA

was synthesized and then purified by ethanol precipitation as indicated in the manufacturer protocol. sgRNAs targeting middle (exon 13) and end region (exon 46) of the *abca7* gene were selected through the CRISPRscan (https://www.crisprscan.org) web tool. Oligo for middle region sgRNA: 5-taatacgactcactataGGATCATGGGTCTGGGCTCAgttttagagctagaa-3 and oligo for end region sgRNA: 5-taatacgactcactata-GGGCAAATCAAAAAGTCCATgttttagagctagaa-3 were prepared based on a cloning-free method. Each sgRNA oligo was used as forward primer in a PCR reaction with gRNA universal tail primer 5-AAAAGCACCGAC TCGGTGCCAC TTTTTCAAGTTGATAACGGACTA-3 as reverse primer. PCR reaction for each sgRNA was set up with a 100 μL reaction volume containing 1X Q5 buffer, 2 μM each primer, 0.2 mM each dNTP, 2 μL Q5 DNA Polymerase (NEB). Amplification was done with an initial denaturation at 95°C for 30 s followed by 40 cycles at 95°C for 10 s, 60°C for 10 s, and 72°C for 10 s, and a final extension at 72°C for 5 min. The PCR products were then purified by PCR purification kit (Invitrogen) and used as template DNA to generate each sgRNA by *in vitro* transcription using MEGAshortscript T7 kit (Invitrogen). The size and quality of the gRNAs were visualized in 3% agarose gel electrophoresis. The mix of sgRNAs and capped mRNA was injected directly into one-cell stage zebrafish embryos. For every embryo, 2 nL solution containing 600 pg Cas9 mRNA and 100 pg sgRNA from each was injected. To confirm the deletion, specific primers binding on the upstream and downstream regions of the gRNA target sites were designed. 10 single 2-day post injection (dpi) embryos were collected individually and each of them was put into a 1.5 mL Eppendorf tube. Genomic DNAs of single embryos were prepared by alkaline lysis method.[103] 3 μL genomic DNA solution from each embryo was used in a 25 μL PCR reaction containing 1X Taq buffer, 2 μM each primer, 0.2 mM each dNTP and 0.5 μL Taq DNA polymerase. PCR fragment indicating the deletion was visualized in 2% agarose gel electrophoresis. Subsequent DNA sequencing confirmed the partial deletion in *abca7* gene. Injected embryos were raised and then 4-month chimeric F0 candidates were crossed to the wild type AB strain fish and their 2-day old embryos were screened by PCR and genotyped by Sanger sequencing. F1 embryos were raised to adulthood (4-month-old) and then were screened by Sanger sequencing following the PCR on the target site of the genomic DNA prepared from their tail fins. In the end, 16 fish having the partial deleted *abca7* gene were identified.

Generation of *npy*^{nw17} mutant zebrafish

To generate *npy* mutant zebrafish, we used the CRISPR/Cas9 system. The Cas9 target site was identified by using the Ensembl (https://www.ensembl.org/; *npy*: ENSDARG00000036222) and CHOPCHOP (http://chopchop.cbu.uib.no/). The selected *npy* single gRNA target was 5′- GGGAGAGGACGCACCTG-3'. The single gRNA was synthesized by IDT (Alt-R CRISPR-Cas9 sgRNA 2 nmol). One-cell stage embryos of *nacre* (*mitfa*^{b692})[104] were injected with a mixture of the single guide RNA (12.5 pg) and Cas9 mRNA (100 pg). Cas9 mRNA was synthesized from the pT3TS-nCas9n plasmid (Addgene, Plasmid #46757) with mMESSAGE mMACHINE T3 transcription kit (Thermo Fisher Scientific). The injected embryos were raised to adult fish (F0). To screen founder zebrafish carrying germline transmitted mutations, F1 embryos outcrossed from F0 and wildtype zebrafish were collected and analyzed by PCR. For genomic DNA (gDNA) extraction, single F1 larvae at 3 dpf were euthanized by overdose of MS222 and transferred to a 1.5 mL tube. Each larva was lysed with 30 μL lysis buffer (25 mM NaOH, 0.2 mM EDTA), then placed on a heating block at 95°C for 30 min. After the incubation, the lysis reaction was neutralized by adding 30 μL neutralization buffer (40mM Tris-HCl, pH 5) to the tubes, which were subsequently vortexed, spun down, and stored at 4°C until use. The target genomic site was amplified using a quantitative PCR machine (Applied Biosystems Instruments). PCR was done on the extracted gDNAs using the following primers: forward primer, 5'-GAAGATGTGGATGAGCTGGGCA-3' and reverse primer, 5'-GCTCACCTCTGCCTTGTTATGAGG-3'. To perform PCR, 5 μL SYBR green master mix (Thermo Fisher Scientific) was mixed with 0.25 μL of forward and reverse primer and 4.25 μL water to make a 10 μL reaction mixture. This reaction was added to a 96 well qPCR plate (Thermo Fisher Scientific) and 0.25 μL of extracted gDNA were mixed with this reaction. The amplified samples were then analyzed based on their melting curves and by gel electrophoresis and compares to wildtype. After the screening process, the *npy*^{nw17} mutant zebrafish carrying a 44-bp deletion was identified. F2 heterozygotes were inbred to generate F3 homozygous *npy* mutants for this study. The deletion leads to a frameshift mutation in the N terminus sequence encoding for the signal peptide. As a result, the mutant *npy* allele encodes for the first 26 amino acid of the *npy* signal peptide (missing the last 2 amino acids) followed by 29 amino acids, that are completely different from the wild type Npy, failing to produce a mature peptide.

Microinjection, tissue preparation, and immunohistochemistry

Cerebroventricular microinjections (CVMI) into adult zebrafish brain were performed as described.[14,15] 8–12 months old *abca7*$^{+/-}$ heterozygous knockouts and their respective age-matched wild type siblings of both sexes were used for the experiments. The animals were injected with the followings: PBS (control), human amyloid-beta42 (Aβ42, 20 μM), human Neuropeptide Y (10 μg/mL), BDNF (100 ng/mL), NGFR inhibitor (NGFRi) LM11A-31 (20 μM). Total injection volume was 0.5–1 μL. At 3 days post injection (dpi), animals were euthanized and subjected to histological tissue preparation. The zebrafish heads were dissected and fixed overnight at 4°C using 4% paraformaldehyde. After few washes the heads were incubated overnight in 20% Sucrose with 20% ethylenediaminetetraacetic acid (EDTA) solution at 4°C for cryoprotection and decalcification. The following day, fish heads were embedded in cryoprotectant sectioning resin O.C.T. and cryosectioned into 12-μm thick sections on SuperFrost Plus glass slides. For immunohistochemistry, the sections were dried at room temperature, followed by washing steps in PBS with 0.03% Triton X-100 (PBSTx). Primary antibodies were applied overnight at 4°C. Next day, the slides were washed 3 times with PBSTx and then appropriate secondary antibodies were applied for 2 h at room temperature. The slides were then washed several times before mounting using 70% glycerol in PBS. Antibodies used are listed in Table S1. For antigen retrieval of PCNA and SV2, slides were heated in

10 mM Sodium citrate (pH: 6.0) at 85°C for 15 min before primary antibody incubation. For antigen retrieval of NPY, slides were heated in 50 mM Tris-HCl (pH:8.0) at 95°C for 5 min before primary antibody incubation.

Single-cell sequencing in zebrafish and data analyses

The telencephalon of the 10-month-old fish (one male and two females per genotype into one biological replicate) were dissected in ice-cold PBS and directly dissociated with Neural Tissue Dissociation Kit (Miltenyi Biotec, Cat. No. 130-092-628) as described previously.[11,105] After dissociation, cells were filtered through 40 μM cell strainer into 10 mL 2% BSA in PBS, centrifuged at 300 g for 10 min, and resuspended in 4% BSA in PBS. Viability indicator dyes Sytox Blue (Invitrogen, Cat No. S34857) and Dycle Ruby (Invitrogen, Cat. No. V10309) were used to sort the cells by FACS. Samples from *abca7* heterozygous knockout and wild type negative siblings were sorted in separate FACS machines (Sony MA900-FP) to ensure as minimum incubation time for the samples placed on ice (Figure S4). The resulting single cell suspension was promptly loaded on the 10X Chromium system.[106] 10X libraries were prepared as per the manufacturer's instructions. Generated libraries were sequenced via Illumina NovaSeq 6000 as described.[10,11,105,107,108] In total, 54,482 cells were sequenced. The raw sequencing data was processed by the Cell Ranger Single Cell Software Suite (10X Genomics, v6.1.2) with the default options. On average, 96.65% of the total 1,70 billion gene reads were aligned to the zebrafish genome release GRCz11 (release 105). The resulting matrices were used as input for downstream data analysis by Seurat.[101]

Read alignment and quality control

The single cell expression matrices were read by Read10X function of Seurat[109] (version 4.1.3) R package (v4.2.2.1). The Seurat objects were created by filtering out the any cells with less than 200 expressed genes, and with genes expressed in less than 3 cells. After filtering out the low-quality cells, Seurat objects were normalized, and the top 2,000 variable genes were used for further analyses. After identifying the anchors (FindIntegrationAnchors), the datasets were integrated (IntegrateData). We used DoubletFinder[110] to identify and remove doublets, and the rest of the analyses were done on singlets. The integrated Seurat object included 50,691 cells with 26,122 genes. The data were scaled using all genes, and 30 PCAs (RunPCA) were identified. Cell clustering, marker gene analyses, differential gene expression and preparation of feature plots were performed as described.[11,24,58,101,111] Resolution of 1 was used to identify the clusters. In total, 35 clusters were identified. The main cell types were identified by using *s100b* and *gfap* for Astroglia; *sv2a*, *nrgna*, *grin1a*, *grin1b* for Neuron; *pdgfrb* and *kcne4* for Pericyte; *cd74a* and *apoc1* for Microglia; *mbpa* and *mpz* for Oligodendrocyte; *aplnra* for OPC; *myh11a* and *tagln2* for vascular smooth muscle cells, *lyve1b* for lymphatic endothelial cells and *kdrl* for vascular cells.[10,11] To find differentially expressed genes (DEGs), we used FindMarkers function of Seurat with 0.25 logfc.threshold, and for GO-term analyses, DEGs were used as described.[11]

Expression analyses in AD cohorts

Analysis of the human AD bulk RNA-seq data has been reported previously.[112,113] To assess differentially expressed genes (DEG) between AD and control, multiple linear regression models were used to compare the conditional-quantile-normalized expression values between AD and control participants while adjusting for covariates including RNA integrity number (RIN), sex, age at death, sequencing flow-cell or batch, tissue source, and participant race, where applicable, followed by multiple testing corrections using false discovery rate. For expression data from the Mount Sinai Brain Bank, AD vs. control DEG was also performed in a subset of non-Hispanic white (NHW) participants. The associations between gene expression and Braak stage were assessed in TCX, CER, and DLPFC, following similar multiple linear regression models where age at death, sex, RIN, sequencing flow-cell or batch, and *APOE-ε4* allele dosage were adjusted. Multiple testing was corrected using false discovery rate. Cell-intrinsic DEG results were retrieved from previously published work.[113] The construction of the WGCNA[114] was described previously.[115] We reported the co-expression modules containing the genes of interest.

The single-nucleus RNA-seq data[19] were generated using frozen postmortem tissue from the temporal cortex of 12 individuals with pathologically confirmed AD[116] cases, and 12 age-, sex-matched control individuals with approval from the Mayo Clinic Institutional Review Board and written informed consent from the participants or their qualified next-of-kin. Briefly, to assess tissue quality, RIN was measured using RNA Pico Chip Assay (Agilent Biotechnologies, 5067-1513) on an Agilent 2100 Bioanalyzer using total RNA extracted from ~20mg of brain tissue. Single nuclei suspension was collected on high-quality tissues (RIN >5.5) using an established protocol with modification.[117] The nuclei were incubated with mouse anti-Human Nuclear Antigen [235-1] (Abcam, ab191181) antibody at 1:200 dilution and sorted using a BD FACSAria II sorter. Single cell RNA-seq libraries were prepared using the Chromium Single Cell 3′ Gel Bead and Library Kit v3 (10X Genomics, 120237) and the Chromium i7 Multiplex Kit (10X Genomics, 120262) according to the manufacturer's instructions. DNA libraries were sequenced at the Mayo Clinic Genome Analysis Core (GAC) using the Illumina HiSeq4000 sequencer.

Raw reads were aligned to human genome build GRCh38 and a premature mRNA reference file. After QC, log-normalization, and clustering of the snRNA-seq data, cluster marker genes were calculated as the genes that are 1) expressed in over 20% AD and control nuclei, 2) overexpressed in the cluster (logFC >0.25), and 3) the Bonferroni-adjusted *p*-value for the overexpression is less than 0.05 based on rank-sum test. The cell types were subsequently assigned based on information from multiple approaches. First, the statistical enrichment of cluster marker genes in a list of marker genes[118] for neurons, astrocytes, oligodendrocytes, endothelial cells, and oligodendrocyte progenitor cells (OPCs) was calculated using hypergeometric tests. The second approach was to check the

existence of well-recognized cell type markers in top cluster markers: *SYT1*, *SNAP25*, *GRIN1* for neurons; *SLC17A7*, *NRGN* for excitatory neurons; *GAD1*, *GAD2* for inhibitory neurons; *VCAN*, *PDGFRA*, *CSPG4* for oligodendrocyte progenitors (OPCs); *MBP*, *MOBP*, *PLP1* for oligodendrocytes; *C3*, *CSF1R*, *CD74* for microglia; *AQP4*, *GFAP* for astrocytes; *FLT1*, *CLDN5* for endothelial cells; and *PDGFRB* for pericytes. Combining the above two approaches and the ScType automated cell type identification,[119] we assigned cell types and subtypes to each cluster.

In silico interaction mapping

NicheNet[120] analysis tool was applied, in a targeted fashion, to study the interaction between *NPY* and its potential target genes in each cluster through NicheNet R package. Prior knowledge of ligand-target interaction has been compiled and optimized by NicheNet from multiple data sources to give a prior model which contains the regulation strength of ligands toward target genes. In this study, we assumed that *NPY* was the ligand based on previous works.[78,82,98,121,122] Further, we required the NPY receptors being the following *NPY1R*, *NPY2R*, *CXCR4*, *NPY4R*, *NPY5R*, or *NPY6R*. For a given cluster that had NPY receptors expressed in it, the predicted target genes of NPY were those that 1) DEGs between AD and control cells, 2) expressed in $\geq$20% cells of the cluster, 3) among the top regulated genes of NPY according to the NicheNet prior model.

Whole-genome sequencing

We analyzed whole-genome sequencing (WGS) in 2,535 individuals from 522 families in EFIGA[71] and AD-FBS cohorts. The NIA AD-FBS is the largest collection of familial AD worldwide.[70] The sequencing was performed at the New York Genome Center (NYGC) as described,[123] using one microgram of DNA, an Illumina PCR-free library protocol, and sequencing on the Illumina HiSeq platform. Variants were called using NYGC automated analysis pipeline which is based on CCDG and TOPMed recommended best practices.[124] Variant filtration was performed using Variant Quality Score Recalibration (VQSR at tranche 99.6%), sample missingness (>2%), depth of coverage (DP < 10) and genotype quality (GQ > 20). We then annotated high quality variants using ANNOVAR for population level frequency using Genome Aggregation Database (gnomAD), in-silico function using Variant Effect Predictor (VEP) and variant conservation using Combined Annotation Dependent Depletion score (CADD).

Rare variant family segregation analyses

We tested segregation of rare, high-risk loss of Function (LoF) and missense variants with CADD score >20 in *ABCA7*, *BDNF*, *NPY* and *NGFR* genes with clinical AD status. We tested segregation in 214 Caribbean Hispanic and 197 non-Hispanic White families with two or more affected members. Variants were defined as completely segregating if present in all affected family members and unaffected carriers must be at least five years younger than the average age of AD onset in families. The details of the family segregation study was documented before.[125]

Human brain DNA methylation measurement

The genome-wide DNA methylation profile was measured by the Infinium MethylationEPIC Kit (Illumina) on New York Brain Bank, NIA AD-FBS/NCRAD and EFIGA cohorts.[71] On the sample level quality control (QC), we have checked the control probes, sex mismatch, contamination, and genotype outlier calling to identify and remove those samples failed any of these QC metrics. On the CpG probe level QC, we kept those CpG sites with detection p value <0.01 across all the qualified samples and mask those sample specific CpG site with new detection $p > 0.01$.[126] We further removed those CpG sites reported to have cross-hybridization problems[127,128] and those polymorphic CpG sites.[128,129] We further corrected the dye bias for all the qualified CpG probes. For this study, we included 20 Hispanic samples with both DNA methylation and GWAS data.

Single-nucleotide polymorphism measurement, mQTL analyses, and Braak stage associations

We measured the genotype of single-nucleotide polymorphism (SNP) across the genome using the Infinium Global Screening Array-24 v3.0 Kit (Illumina) with the same extracted DNA samples used for the DNA methylation measurement. We have conducted the SNP level QC by removing those with missing value > 5% and failed Hardy-Weinberg Equilibrium (HWE) test. As a result, there remained 4 SNPs at *ABCA7* loci, which were included into the mQTL analysis. For each of the 4 extracted SNPs at *ABCA7* loci, we conducted generalized linear regression model by treating the methylation of CpG sites at *ABCA7*, *NPY*, *BDNF*, and *NGFR* as dependent variables and genotypes of the 4 SNPs as independent variables with the adjustment of age, sex, ethnicity, and technical covariates. Those CpG sites with p value <0.05 were considered as significant loci. New York Brain Bank, NIA-LOAD/NCRAD and Mayo Clinic Jacksonville cohorts[71] were used.

ABCA7 knockout patient iPSC-derived neurons

The neural progenitor cells for *ABCA7* wild-type and knockout[49] were induced into neurons from iPSCs (MC0192; female, 83 years old[49]) using STEMdiff forebrain neuron differentiation kit (08600, Stemcell Technologies) and STEMdiff Forebrain neuron maturation kit (08605, Stemcell Technologies). Neurons were treated with 1 μg/mL of β-amyloid 1–42 peptide (ab120301, Abcam) for 6 weeks. Total RNA was isolated using Trizol and RIPA containing protease inhibitor. The cDNA was synthesized using SuperScript III reverse transcriptase (18080051, Invitrogen). Real-time PCR was performed with SYBR Green Supermix (1725271, Bio-Rad) and relative gene expression was normalized to *GAPDH* expression and assessed using the $2^{-\Delta\Delta CT}$ method. Primers used in this study were

as follows (all 5′to 3′): *GAPDH*: forward: GTCTCCTCTGACTTCAACAGCG, reverse: ACCACCCTGTTGCTGTAGCCAA; *ABCA7*: forward: CCTTGCACAGCTTGTTGGAG, reverse: CTGCTAGGTCCCCTGACACT; *NPY*: forward: CGCTGCGACACTACATCAAC, reverse: CTCTGGGCTGGATCGTTTTCC; SLC17A7: forward: CTGGGGCTACATTGTCACTCA, reverse: GCAAAGCCGAAAACTC TGTTG; GAD1: forward: GCGGACCCCAATACCACTAAC reverse: CACAAGGCGACTCTTCTCTTC. Immunolabeling of iPSC derived neurons were performed as described[49] by using MAP2 monoclonal antibody (MAB3418X, clone AP20, Chemicon; 1:400 dilution).

Human brain sections and immunohistochemistry

Human brain sections from BA9 prefrontal cortex were also obtained from the New York Brain Bank at Columbia University (two individuals with Braak stage IV/V, two individuals with Braak stage I/II) and immunohistochemical stainings for NPY and BDNF were performed as described.[17,130]

NGFR blockage

LM11A-31 dihydrochloride (CAS Number: 1243259-19-9) a non-peptide $p75^{NTR}$ ligand that selectively competes with pro- and mature forms of neurotrophin binding to $p75^{NTR131}$ was purchased from MedChemExpress (HY-11015). A stock solution of 1 mM was prepared using phosphate buffer saline (PBS) pH = 7.4, and further diluted to final concentration of 20 μM in 400 μL E3 buffer solution. The efficacy of LM11A-31 was tested on Tg(NF-κB:GFP) zebrafish embryos.[100] 3 dpf zebrafish embryos ($n = 4$ per condition) were randomly selected and immersed in 24-well plates (Thermo Scientific, 142475) (400 μL per well). Vehicle-treated control embryos were similarly treated with 8 μL of PBS. The well plate was placed into the incubator (BINDER GmbH, Germany) at 28°C. After each 24 h of incubation period the drug solution was replaced by fresh solution. After drug incubation time, larvae were transferred to a 50 mm glass-bottom dish (P50G-1.5-14-F MatTrek Co, USA) and sedated with 0.001% Tricaine (Sigma Aldrich, A5040) in E3 buffer solution. Visualization of GFP was performed using Zeiss LSM800 confocal microscope equipped with ZEN software (version blue edition, v3.2, Carl Zeiss, Jena, Germany). Imaging focus was made on tail region of zebrafish embryo to minimize rotational differences. The fluorescence intensity measures were performed using integrated ZEN measurement tool. GraphPad Prism software version 9.2.0. was used for the statistical analyses.

ELISA measurements

To measure the NPY level in the brain, we dissected brains, snap-frozen in liquid nitrogen and stored at −80°C. For protein isolation, brains were lysed and homogenized with RIPA buffer containing protease inhibitors. Protein concentration was determined by using BCA assay (Pierce). Tissue concentrations of NPY in protein lysates were measured by using commercially available enzyme-linked immunosorbent assay (ELISA) kit (EZHNPY-25K, Millipore, USA), following the manufacturer's instructions with a lower limit of detection of 2 pg/mL. Three technical replicates were used for analyses. The absorbance was read at 450 nm in BioTek ELx800 (BioTek Instruments) plate reader within 5 min. We used linear regression to obtain sample concentrations.

QUANTIFICATIONS AND STATISTICAL ANALYSIS

Image quantifications and ELISA measurements

Images were acquired using a Zeiss confocal LSM800 microscope in a 20X or 40× objectives with tiles/z stack function wherever necessary. 6 telencephalon sections between the caudal end of the olfactory bulb and anterior commissure were used per animal for the quantitative analyses ($n \geq 3$ animals in every experimental group). The quantification of SV2-positive synapses was performed using 3D object counter module of ImageJ software with a same standard cut-off threshold for every images. For quantification of microglia, the number of cells immunoreactive to L-plastin were counted. For quantification of PCNA+GS double-positive cells, overlap of PCNA-positive nuclei with GS-positive cell were counted. Image acquisition was performed in a blinded fashion. The statistical analyses were performed using GraphPad Prism (Version 9.5.1) for one-way ANOVA followed by a post-test depending on the data structure (Sidak's multiple comparison test, Tukey's multiple comparison test, Dunnett's multiple comparison test, Brown-Forsythe and Welch post-test with two-stage linear step-up procedure of Benjamini, Krieger and Yekutieli, or non-parametric Kolmogorov-Smirnov test) wherever applicable. Tests used are indicated at respective figure legends. Error bars shown are the SEM and asterisks indicate significance according to: *: $p < 0.0332$, **: $p < 0.0021$, ***: $p < 0.0002$, ****: $p < 0.0001$; not significant (n.s.: $p > 0.0332$). For ELISA measurements, parametric t test was used for statistical analyses.

Braak stage associations

For association between brain RNA expression and Braak stage, we conducted generalized linear regression model Braak∼Age+Gender+Gene_A+Gene_B+ Gene_A*Gene_B+ RACE+cohorts+PMI+RIN) with binary Braak stage categories (Braak 0–4 and Braak 5–6) with the adjustment of age, sex, ethnicity, postmortem interval (PMI) and RIN number for RNA quality as technical covariates.

Repeated measurements

No repeated measurements were taken on one sample.